26

Combined Endoscopic Optical Coherence Tomography and Laser Induced Fluorescence

J.K. Barton, A.R. Tumlinson, and U. Utzinger

26.1 Introduction

Optical coherence tomography (OCT) and laser induced fluorescence (LIF) are promising modalities for tissue characterization in human patients and animal models. OCT detects coherently backscattered light whereas LIF detects fluorescence emission of endogenous biochemicals such as reduced nicotinamide adenine dinucleotide (NADH), flavin adenine dinucleotide (FAD), collagen, and fluorescent proteins, or exogenous substances such as cyanine dyes. Given the complimentary mechanisms of contrast for OCT and LIF, the combination of the two modalities could potentially provide more sensitive and specific detection of disease than either modality alone. Sample probes for both OCT and LIF can be implemented using small diameter optical fibers, suggesting a particular synergy for endoscopic applications. In this chapter, the mechanisms of contrast and diagnostic capability for both OCT and LIF are briefly examined. Evidence of complimentary capability is described. Three published combined OCT-LIF systems are reviewed, and existing and potential endoscope designs are illustrated.

26.2 Background on Optical Coherence Tomography

OCT provides high-resolution, depth resolved images of scattering tissues. With micron scale resolution and millimeter depth of imaging, OCT is ideal for examining superficial and optically accessible tissues. Most commonly, the amplitude of the backscattered signal is displayed to yield structural images. In this case, signal originates from index of refraction mismatches. Functional variants described in elsewhere this handbook include polarization sensitive OCT, which is sensitive to tissue birefringence and optical axis orientation [1–5]; Doppler OCT, which measures the velocity of moving scatterers, [6–9]; phase contrast OCT, which is sensitive to small changes in optical pathlength [10–12]; and molecular contrast OCT (MCOCT) [13, 14], which

includes measurement of changes in the source spectrum due to attenuation by endogenous or exogenous substances [15, 16], as well as detection of processes that yield coherent radiation, e.g. coherent anti-Stokes Raman scattering [17] and second harmonic generation [18, 19]. Several exogenous scattering agents have also been proposed to selectively enhance the OCT signal [20–23]. These additional mechanisms of contrast may augment the diagnostic capability of OCT. MCOCT, similar to LIF, has the potential to identify and quantify the presence of certain endogenous and targeted or untargeted exogenous molecules.

26.2.1 Diagnostic accuracy of Optical Coherence Tomography

OCT has demonstrated promise for providing accurate diagnoses in a variety of organ sites. Several clinical applications are described in detail in this handbook. Diagnosis and management of retinal disorders, early cancer detection (especially in epithelial tissues), and detection of vulnerable plaque are perhaps the most widely studied applications. The number of large scale clinical studies performed to assess diagnostic accuracy of OCT is currently modest. The results of five *in vivo* and *ex vivo* human studies, each using histology as the gold standard, are summarized below. Sensitivity is the fraction of abnormal samples correctly classified and specificity the fraction of normal samples correctly classified.

1) *Esophagus*: The performance of endoscopic OCT for the diagnosis and exclusion of dysplasia in patients with Barrett's esophagus was evaluated *in vivo* in 33 patients. Results were: sensitivity, 68%; specificity, 82%; positive predictive value, 53%; negative predictive value, 89%; and diagnostic accuracy, 78%. Diagnostic accuracy for the 4 endoscopists ranged from 56% to 98% [24].
2) *Urinary Bladder*: Endoscopic OCT was used *in vivo* in 24 patients at high risk for transitional cell carcinoma of the bladder. OCT had a sensitivity of 100%, specificity of 89%, positive predictive value of 75%, and negative predictive value of 100%. The accuracy was 92% [25].
3) *Artery*: Human autopsy artery segments (n = 357) were visualized with OCT and compared to histology. With two readers, sensitivity and specificity ranged from 71% to 79% and 97% to 98% for fibrous plaques, 95% to 96% and 97% for fibrocalcific plaques, and 90% to 94% and 90% to 92% for lipid-rich plaques, respectively (overall agreement, kappa = 0.83 to 0.84). The interobserver and intraobserver reliabilities of OCT assessment were high (kappa values of 0.88 and 0.91, respectively) [26].
4) *Colon*: Colectomy specimens from patients with diagnosis of Crohn's disease (n = 24) and ulcerative colitis (n = 24) were imaged with OCT and compared to histopathology. The sensitivity and specificity for OCT to detect transmural disease were 86% and 91%, respectively [27].
5) *Pancreas*: Surgical specimens of pancreas were examined and images of the main pancreatic duct obtained. OCT had a sensitivity and specificity for

discrimination between adenocarcinoma and normal tissue of 78.6% and 88.9%, respectively. However, OCT images of dysplasia and inflammation were more often then not similar to normal tissue [28].

While these studies have demonstrated that OCT can provide good to excellent diagnostic accuracy, the referenced authors and others have pointed out limitations. First, clinically practical endoscopic OCT systems have limited resolution. Lacking subcellular resolution, identification of cell types or visualization of markers of neoplasia such as abnormal nuclear size is not directly possible (although statistical image analysis may reveal certain cellular attributes). Even ultrahigh resolution OCT systems cannot generally visualize subcellular structure at depth in highly scattering human tissue. Given reliance on tissue architecture features for diagnosis, benign conditions such as scarring may be confused as pathology. OCT images also suffer from speckle, which can obscure features and boundaries.

26.3 Background on Laser Induced Fluorescence

Fluorescence is radiative emission following stimulation of a molecule into an excited state [29]. Fluorescence is characterized by the absorption properties of the molecule, the lifetime of the excited state, the ratio of the radiative versus non-radiative decay rates (quantum yield) and the structure of the vibrational levels of the ground state (emission spectrum). The fluorescence emission spectrum usually is independent of the excitation wavelength and is red shifted compared to the excitation. The emission spectrum is often a mirror image of the excitation spectrum, separated by the Stokes shift, because the structure of the vibrational levels is similar for the excited and the ground states. Fluorescence spectroscopy contains more information about the molecule's environment than does absorption spectroscopy. For example, upon polarized excitation, small fluorescence molecules exhibit more unpolarized emission compared to large molecules or molecules bound to rigid structures because the fluorescence lifetime limits the reorientation time of the molecule before emission. The fluorescence intensity can be quenched through static and dynamic pathways. Static pathways form new, less-fluorescent molecules through chemical reactions with the quencher and dynamic pathways increase non-radiative decay rates through collisions with the solvent. If two fluorescent molecules are in close proximity and their emission and absorption spectrum overlap, energy transfer can occur from the donor molecule to the acceptor (Foerster Resonant Energy Transfer), making the emission characteristics dependent on the distance between the two molecules. The transfer efficiency between the donor and acceptor can also be measured through a decrease of the lifetime of the donor. Fluorescence emission is incoherent thus will not produce speckle.

26.3.1 Fluorophores

Fluorescence in living tissue originates from endogenous fluorophores but can also be introduced by exogenous contrast agents or generated in genetically modified species expressing fluorescence proteins or enzymes capable of activating chemiluminescence. Endogenous fluorescence can be excited from intracellular constituents such as metabolites and proteins as well as interstitial components such as structural proteins. Several reviewers have discussed the application of endogenous fluorescence and surveyed the biologic fluorophores [30–35]. Endogenous fluorophores in tissue are available at concentrations in the range of micromolar to hundreds of nanomolar. Their relatively low concentration and preferred excitation at short wavelengths suggests that they may not be amenable to interrogation by MCOCT. In general, endogenous tissue fluorescence with excitation below 300 nm is approximately an order of magnitude stronger than with UV-A (320–400 nm) excitation, and fluorescence emission with blue excitation is approximately another order of magnitude weaker than with UV-A excitation. Proteins are responsible for the high fluorescence efficiency of tissue excited below 300 nm because many proteins contain the aromatic amino acids tyrosine, tryptophan, and phenylalanine [29].

Landmark studies have established a link between cellular metabolism and fluorescence emission [36–38]. Key fluorophores that correlate specifically with cellular activity include the electron carriers NAD and FAD. As a cell changes its metabolic activity, the balance between the reduced (NADH, $FADH_2$) and oxidized (NAD, FAD) form of the electron carrier shifts correspondingly as the reduction-oxidation (redox) state of the cell fluctuates. Because only NADH and FAD exhibit significant fluorescence signals, the redox state can be estimated through a ratio of the peak emission values from these molecules assuming their concentrations are inversely linked to the nonfluorescing counterparts.

Type I collagen, one of the main components of the interstitial matrix, exhibits both optical scattering and autofluorescence, two properties that can potentially be exploited as a diagnostic marker of the interstitial matrix using both OCT and LIF. Significant fluorescence has also been noted from elastin fibers and keratin.

Fluorescence emission in the red was observed in animal sarcomas in the beginning of the 20^{th} century using a Wood's lamp [39] and later confirmed to originate from porphyrins [40]. There may be multiple sources of porphyrins in tissue, such as incomplete heme-synthesis, microbes, or a by-product of some tumors [41, 42]. Additionally, the authors have shown that a chlorophyll rich diet increases emission from the colon at 680 nm, which is consistent with the spectral profile of chlorophyll and its metabolites such as pheophorbide-*a* and pyropheophorbide-*a* [43, 44], making chlorophyll in diet an important exogenous fluorophore in the colon.

Current contrast agent developments in molecular imaging can increase the visibility of molecular phenotypes, even though the target of interest might not exhibit itself a strong optical signature. Fluorescence based reporters can be detected in very low quantities (picomolar, compared to 10's of micromolar reporter concentration currently needed for MCOCT). Several exogenous compounds have been approved for *in vivo* clinical applications, e.g. visualization of the ocular vasculature with fluorescein or indocyanine green (ICG). Those compounds are intravenously injected and made available as systemic fluorescent substrate. Semiconductor nanocrystals compared to conventional fluorophores have relatively narrow and tunable emission spectra and are photochemically stable.

Protoporphyrin IX is an end product of metabolized delta-5-aminolevulinic acid (ALA) and ALA is thought to preferentially accumulate in tumors. Over the last 5 years several studies have evaluated ALA induced fluorescence for skin cancer detection [45,46], colon cancer [47–49], larynx [50] and the bladder [51–53]. The measurement of ALA induced fluorescence is compatible with combined OCT-LIF devices.

26.3.2 Diagnostic Accuracy of Laser Induced Fluorescence

Fluorescence spectroscopy has been proposed for the assessment of patients at increased risk for developing a disease, for demarcation and identification of lesions, and for prognostic follow-up after treatment. Early reports suggested that quantitative endogenous fluorescence could discriminate between normal and malignant tissues [54]. In the 1980s Alfano and coworkers reported endogenous fluorescence measurements *in vitro* [55] and subsequently, through the advancement in fiberoptic light delivery and detection as well as the development of sensitive and portable spectral analyzers, a multitude of clinical and pre-clinical endogenous tissue spectroscopy studies have been conducted. Recent review articles summarize the chronological evolution and diagnostic performance of LIF up to the year 2000 [56] and summarize spectroscopic detection of neoplasia [57]. Clinical studies have been performed in the colon, cervix, bronchus, bladder, brain, oral cavity, larynx, skin, bile duct, breast, arteries and stomach. Here we summarize recent results for several organ sites in Table 26.1. When available, performance of current clinical visual examination is also reported (* in Table 26.1). As with OCT, the diagnostic performance of LIF is highly variable but generally ranges from good to excellent. Recent significant studies in the two most published organ sites are described in additional detail below:

1) Cervix: Accurate optical diagnosis of cervical dysplasia could lead to a method where patients with an abnormal cytological screening result are triaged into those who do not need any further intervention and those who need a biopsy or potentially a treatment in the same visit. Several groups have reported recent results including a multi center clinical trial

Table 26.1. Sensitivity and specificity obtained in select LIF clinical studies. Where available, sensitivity and specificity for a standard clinical method is given also in parentheses. Abbreviations: Bx: biopsy, ex: excitation, hg: high grade (moderate/severe dysplasia and cancer) versus non high grade, mc: multicenter study, MIT: Massachusetts Institute of Technology, NA: information not available, SIL: squamous intraepithelial lesion, trim: trimodal spectroscopy, UT: University of Texas at Austin, UW: University of Wisconsin Madison, VU: Vanderbilt University, wl: white light

Organ Site	# Subjects/ samples	Sensitivity	Specificity	Source (year, reference, organization, ex. wavelength/notes)
Cervix,	604/1,500	92% (*67%)	50% (*54%)	2004, [58] Medispectra, 337, MC, hg
*colposcopy	147/351	71%	77%	2002, [59] UT, multi ex, hg
	44/84	92%	71%	2002, [60] MIT, trim, SIL-Bx. nonSIL
	95/381	79% (*79%)	78% (*76%)	1996, [120] UT, 337, 380, 460, hg
Lung,	1173/1978	82.3% (*57.9%)	58.4% (*62%)	2005, [67] Storz, mc, hg
*wl bronchoscopy	32/62	80%	83%	2004, [69] Olympus
	173/864	67% (*25%)	66% (*90%)	1998, [66] Xillix, mc, hg
Oral cavity,	4/4 (images)	91% (*75%)	86% (*43%)	2005, [121, 122] UT, visual
*wl examination	15/91	96%	96%	2003, [123] MIT, trim.
	76/343	100% (*100%)	88% (83*)	2002, [124] UT, multi ex
Breast	18/47	54%	91%	2005, [125] UW, multi ex
	32/56	70%	92%	2003, [126, 127] UW, multi ex
	63/911	99%	99%	1997, [128] 337
Colon	NA/177	80%	92%	1992, [129] Wellman, 337
Barret's	37/148	74%	85%	2003, [130] Wellman, 400
esophagus	53/141	76%	63%	2003, [131] Lausanne, 505
Bladder	75/130	95%	73%	1998, [132] Wellman, 337
Brain	26/120	100%	76%	2001, [133] VU, primary tumor
		97%	95%	2004, [134] data from [133]

by MediSpectra [58] with a single wavelength excitation source combined with diffuse reflectance measurements. The report indicated a 33% increase in detection rate for high grade disease while maintaining the specificity at the level of current clinical practice. In 2002 Chang and co-workers [59] as well as Georgakaudi and coworkers [60] published results of their studies on 147 and 44 patients respectively. Chang reported that more than 3–4 excitation wavelengths do not improve performance and confirmed previous findings by Ramanujam [61]. He also reported low performance in detecting low grade disease and distinguishing normal columnar tissue from high grade disease. Georgakaudi reported results using an analytical model for extracting intrinsic fluorescence [62], reduced scattering and absorption [63], as well as estimates for average number and size of main scatterers [64]. Sensitivity was significantly improved when a combined trimodal approach was used while the specificity was maintained.

2) Lung: The LIFE fluorescence endoscopy systems from Xillix uses excitation between 380 and 460 nm emission and observes fluorescence in the green and red [65,66]. The D-Light system from Storz incorporates an additional white light measurements [67] and the AFI system from Olympus utilizes two additional reflectance channels at 550 and 610 nm [68,69]. A European multi center trial with the D-Light system reported increased sensitivity [67] compared with the earlier multi center trial by Lam et al. [65] with the Xillix system and corrected the sensitivity and specificity of white light bronchoscopy reported by Lam. The AFI system was tested on a small sample size and only abnormal appearing sites were included in the analysis [69]. A relatively high false positive rate was reported which limits the positive predictive value [70] and difficulties in distinguishing pre-invasive lesions and benign conditions were mentioned.

26.4 Advantages of a Dual Modality System

The complimentary nature of information provided by OCT and LIF (coherent backscatter versus incoherent fluorescence emission) creates the possibility that the combination of OCT and LIF may be more sensitive to tissue function and pathology than either modality alone. The two types of information may also facilitate signal interpretation and increase specificity. Viewing this potential advantage from two different perspectives, cross-sectional OCT images may help to correct and interpret LIF spectra, or LIF imaging/spectra may help to guide and interpret OCT images.

From the first perspective, LIF spectra may be difficult to interpret because they may be influenced by unknown subsurface structures. Spectra obtained at different lateral locations on an apparently smooth, homogeneous surface can vary in intensity and spectral shape. Without depth resolved anatomical information, it may be difficult to determine if the variation is due to changes in tissue function, type, or thickness. For example, in a layered epithelial/stromal

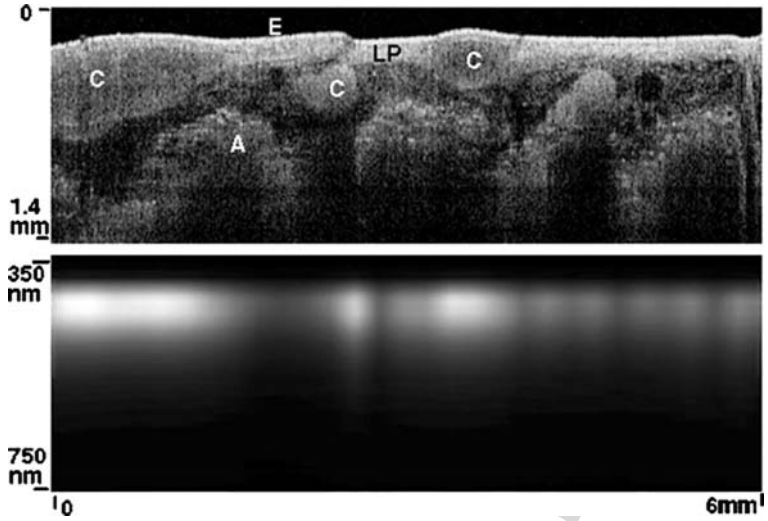

Fig. 26.1. OCT image (*top*) and LIF spectra (*bottom*) of excised sheep lung bronchus. Note the increase in emission intensity at lateral locations corresponding to subsurface cartilage (C). Other abbreviations: epithelium (E), lamina propria (LP) alveoli (A)

tissue, a relative decrease in the intensity of the fluorescence signal associated with collagen could be due to a true lessening of the fluorescence emission of the stroma, or could be caused by a thickening of the overlying epithelium. Another example is given in Fig. 26.1. An OCT image/LIF spectra pair is shown, obtained from the luminal surface of an approximately 3 mm diameter bronchus of excised sheep lung. The spectral shape of the LIF signal is relatively constant, but the intensity is highly non-uniform. The OCT image shows clearly that strong LIF signal corresponds to locations with subsurface cartilage, indicating that the LIF intensity variation is due to normal anatomy.

Quantitative measures of tissue anatomy obtained with OCT can be used to correct LIF data. Several attempts have been made to separate tissue optical properties such as scattering, absorption and intrinsic fluorescence from extrinsic fluorescence, and to calibrate fluorescence measurements for illumination and detection conditions. The collected fluorescence depends on optical transport within the tissue [70, 71] and geometrical sensor sample relations [72–74]. LIF intensity is highly dependent upon the probe-sample separation and OCT can provide this geometrical information with high accuracy. In fact, if only point LIF measurements are being obtained, only a-scan OCT capability is needed. The authors have not found any published articles using OCT to correct for LIF probe-sample separation, but a correction algorithm has been described by Warren et al. [75] using ultrasound a-mode data. A model of the fluorescence intensity was developed and verified with both Monte Carlo simulations and empirical data. A correction equation goes

as $S_c = S_m/R^n$, where S_m is the measured fluorescence intensity, R is the probe-tissue separation, and $n = 1.1$ for aorta and 2 for theoretical, isotropic fluorescence emission.

Using mathematical models, the particular photon traveling paths can be predicted with *a priori* knowledge of the illumination and collection geometry, a diffuse reflection measurement, and assumptions about scattering and absorption properties. Zhang and coworkers developed a method that allows extraction of intrinsic fluorescence in semi-infinite media based on fluorescence and diffuse reflectance measurements under the same geometrical configuration [76], which subsequently has been used in several clinical studies as an analytical model. Sung et al. developed a similar analytical approach for two-layered tissue to predict intrinsic fluorescence from the stroma and epithelium separately [77]. This model depends on the epithelial thickness, a number that can be easily obtained with OCT.

From the second perspective, LIF imaging can guide OCT measurements. OCT provides a microscopic view and thus in many applications complete screening of the area of interest is impractical, necessitating a guidance technique. LIF imaging, which commonly has high sensitivity but low specificity, can be an ideal method to identify regions of interest for OCT imaging. For example, McNichols et al. [78] developed a large diameter ($\sim$1.5 cm) rigid endoscopic probe to detect oral cancer that used autofluorescence imaging as a method of rapidly identifying suspicious regions to subsequently inspect with OCT for more definitive morphological information. More detailed information on this probe is given later in this chapter.

Additionally, LIF has the potential to clarify inconclusive OCT scans. For example, Kuranov et al. [79] used OCT and LIF to image neoplasms in the cervix and found that these two modalities combined produced fewer false positive results than either modality alone: abnormally increased fluorescence due to inflammatory reactions was clearly differentiated from cancer by OCT; conversely, OCT-detected atypical structure could be clarified with LIF to simply be a mature scar.

An evaluation of the diagnostic capability of OCT, fluorescence imaging, and white light imaging separately and in combination has been performed by Wang et al., [80] looking at rat bladders. These authors examined transitional cell carcinoma (TCC) induced by methyl-nitroso-urea. At various time points, the excised bladders were opened and mounted on a ring holder, then investigated with 5-ALA induced fluorescence, cross-sectional OCT, and white light imaging. The authors showed that adding OCT to 5-ALA fluorescence significantly improved specificity (from 53% to 93%) and also increased sensitivity (79% to 100%). OCT alone had a sensitivity of 100% and specificity of 81% for TCC. OCT brought about an increase in specificity primarily because of hyperplastic lesions, which were frequently highly fluorescent, but were usually correctly identified with OCT because the urothelium was thickened but had low, not high backscattering. The increase in sensitivity came from papillary TCC that did not enhance on fluorescence images but clearly had

thickened, highly backscattering urothelium in OCT images. The addition of white light imaging further increased specificity to 93%. This increase was due to squamous hyperplastic or metaplastic lesions, which showed both enhanced fluorescence and thickened, highly backscattering urothelium on OCT images, but which could be correctly identified with white-light imaging.

26.5 Instrumentation Design Considerations

Combined OCT/LIF systems can be essentially two separate systems simply physically packaged together at the tissue location, or can share optical and mechanical parts, light sources, and/or digital processing components. There are many possible variations; here we list some of the design considerations and some current/possible implementations. Design considerations for system combination include the type of OCT and LIF systems desired (e.g. full field or scanning OCT, point or imaging LIF), the spectral range of the light source(s) and LIF emission, the choice of endoscope materials, and safety. General optical design considerations are also discussed.

26.5.1 OCT and LIF systems

Because various types of OCT systems are discussed in detail elsewhere in this handbook, they will not be discussed here. In general, LIF capability can be added to any type of OCT system, although the sharing of components is facilitated if the scan types are common (e.g. both 1, 2 or 3 dimensional scanning or both full field). An appropriate method of signal separation (spectral, temporal or spatial) is required.

Steady state LIF measurements require a light source with a well defined output spectrum, a conduit to transport the excitation light to the sample, illumination and collection optics, and a conduit to transport the emitted light back to a spectral analyzer for optical detection. Instrumentation for fluorescence measurements is well described by Lakowicz [29] and here we focus on spectral compatibility and common *in vivo* measurement limitations.

One of the major challenges in fluorescence detection is the signal to background ratio. Background signals are caused by instrument autofluorescence (see *Materials* section), out of band illumination from the light source, and scattering within the spectral analyzer. Because endogenous signals can be weak, background signals need to be avoided. Out of band illumination suppression should reach 10^{-5} or 10^{-6} for endogenous tissue fluorophore measurements, especially in excitation ranges where the fluorescence efficiency is low (blue to green). Because the amount of collected instrument background is also dependent on the sample reflectivity, traditional subtraction of the sample signal by the instrument response to a negative standard (e.g. a measurement in water) has its limitations. As a rule of thumb, instrument background should be kept below 10–30% of the sample signal. Traditionally, illumination

and collection paths have been constructed separately [81] to reduce system auto fluorescence. Irradiance levels on excitation optics are significantly higher than on collection optics making it necessary to incorporate auto-fluorescence reduction techniques in the illumination conduit and optical elements at the endoscope tip. In typical applications, the collection conduit will receive a significant amount of excitation light backscattered by the sample. If the stray light suppression capabilities of the detection system are exceeded (a spectrograph might have 10^{-4} suppression), the backscattered excitation light can also contribute to the signal background. This can be avoided by dampening excitation light in the detection path with long-pass filters before the emitted light is spectrally analyzed.

26.5.2 Spectral Range of LIF Sources and OCT Sources

For LIF, short-arc lamps have been used as a standard low-cost excitation source when coupled to an excitation monochromator or dielectric band-pass filters. Example radiance data for Mercury-Xenon and Xenon lamps are shown in Fig. 26.2, top panel. Their broad emission range allows wavelength tunability but a common disadvantage of short-arc lamps is the limited ability to focus light into small optical fibers. A large variety of laser modules has been developed for confocal microscopy and most of these lasers are compact and sufficiently transportable for endoscopic fluorescence measurements. Example sources are shown in Fig. 26.2 and abbreviated as XeCl: Xenon Chloride (308 nm emission), HeCd: Helium Cadmium (325 nm), N2: Nitrogen (337 nm), Ar: Argon (351, 364, 458, 488 & 514 nm), Yag: Neodynium Yag (1064, 532 nm), HeNe: Helium Neon (543, 633 nm). Because of the small Stoke's shift of most fluorophores, narrowband sources are preferred to enable efficient collection efficiency of emission light and rejection of excitation light. In contrast, OCT sources are by necessity broadband, with spectral widths of 10's to 100's of nanometers. Also, OCT sources are generally centered in the NIR, to enable greatest depth of imaging in highly scattering tissue. The light source emission spectra for some OCT sources (short pulsed lasers and superluminescent diodes) are shown in Fig. 26.2. Also shown in Fig. 26.2 is the extinction spectrum of three tuned nanoshells (exogenous scattering agents) [82].

26.5.3 Excitation and Emission and Range of Fluorophores

Epithelial tissues usually exhibit a strong fluorescence peak at 280 nm excitation and 350 nm emission, which is associated with tryptophan fluorescence (Fig. 26.2, bottom panel, Cell emission at 280 nm excitation). Cells excited at UV-A wavelengths show strong fluorescence from NADH, which has a maximum at 350 nm excitation and 450 nm emission (Fig. 26.2, cell emission at 350 nm excitation), whereas the oxidized form NAD is not fluorescent [29]. Conversely, FAD fluoresces at a maximum at 450 nm excitation (blue) and 535 nm emission (Fig. 26.2, cell emission at 450 nm excitation), whereas

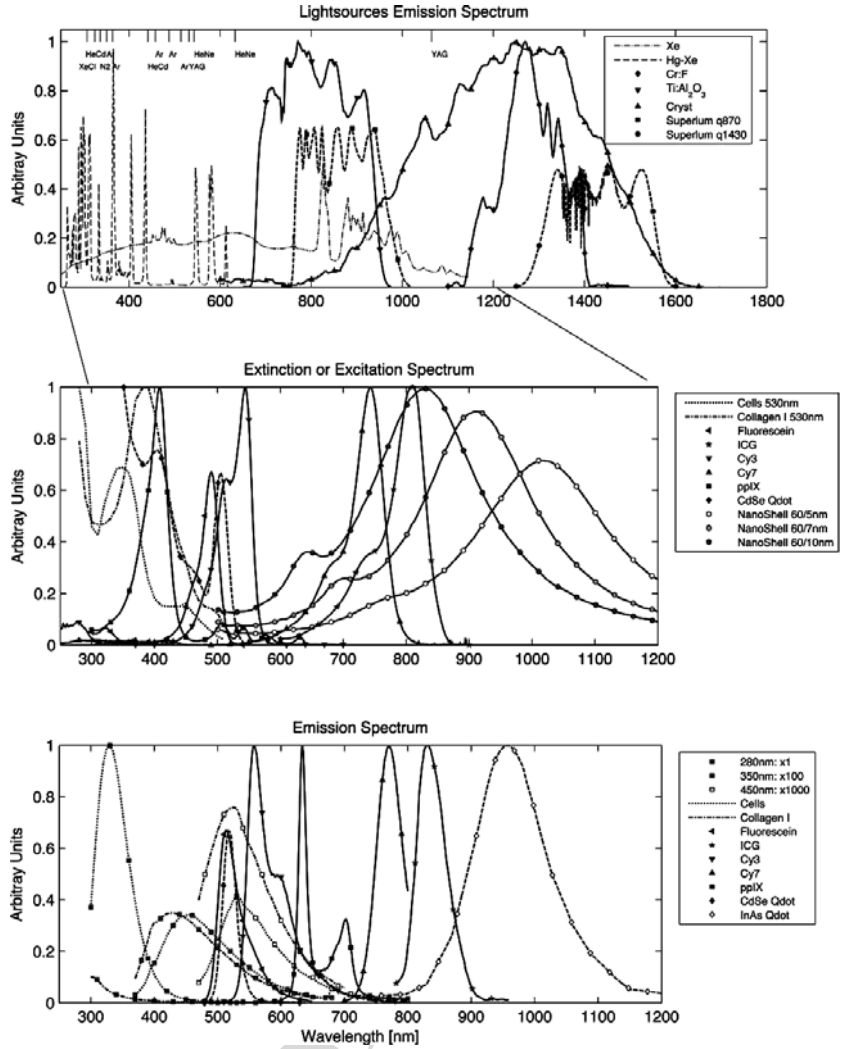

Fig. 26.2. Common light sources, absorbers, and emitters for combined OCT and LIF: *Upper panel*: Illustration of common fluorescence excitation and OCT light sources. Xenon (Xe) and Mercury-Xenon (Hg-Xe) short arc lamps are illustrated (courtesy Photon Technology International, Inc.). Published data from OCT sources using titanium sapphire ($Ti:Al_2O_3$) laser [135], Chromium:forsterite (Cr:F) [136] and photonic crystal fibers (Cryst) [137] as well as emission spectra from commercial superluminescent diodes (Superlum Broadlighters q870 and q1430) are shown. *Middle panel*: Excitation spectra at 530 nm emission are shown for an epithelial cell suspension (OVCA 430) [138] and reconstituted collagen type I. The absorption of fluorescein (Molecular Probes/Invitrogen, 1300ph9) is compared to a semiconductor nanocrystal [139, 140]. ICG, a clinically used NIR absorber, is illustrated as well as protoporhyrin IX (ppIX) [141]. Cyanine dye absorption is illustration with examples of Indocarbocyanine (Cy3) and Indotricarbocyanine (Cy7) [141].

the reduced form $FADH_2$ fluoresces minimally. Fluorescence from interstitial matrix is dominated by collagen; average fluorescence emission from polymerized collagen that was reconstituted from rat tail type I fragments is shown in Fig. 26.2 middle and bottom panel. Typical emission at 280 nm excitation 300 nm emission (consistent with tyrosine), 320 nm excitation/400 nm emission (consistent with the enzymatic crosslinks lysyl hydroxypyridoxyline and hydroxylysyl hydroxypyridoxyline) and 370 nm excitation 450 nm emission (consistent with non-enzymatic crosslinks vesperlysine or crossline) can be observed. Unfortunately, at may excitation wavelength these collagen emission spectra overlap with the emission observed from cell suspensions. Porphyrins show an excitation maximum at 410 nm and two emission maxima at 630 nm and 690 nm while the peak at 630 nm is substantially more intense (Fig. 26.2, protoporphyrin IX). Emission spectra from exogenous fluorophores fluorescein, cyanine dyes Cy3, Cy7, and ICG, and CdSe/InAs quantum dots are also shown in Fig. 26.2. Some of these agents have NIR excitation and/or emission.

Figure 26.2 illustrates that endogenous fluorescence, targeted fluorescence imaging and optical coherence tomography can be spectrally incorporated because most endogenous components do not absorb or emit within the OCT illumination spectral range and some exogenous agents are available outside that range. If spectral overlap occurs, LIF and OCT need to be time or spatially multiplexed. Spectral overlap has been used to advantage in one application [83], with simultaneous OCT/ICG imaging in the eye's fundus. In this case, the same superluminescent diode (793 nm center wavelength, 22 nm spectral full width half maximum) was used for OCT imaging and for excitation of ICG. The key in this implementation was proper selection of the dichroic filter separating backscattered source light (directed to the OCT detector) from fluorescence emission (directed to the LIF detector). This selection minimized distortion of the source correlation function and maximized collection efficiency of fluorescence emission. Excellent simultaneous OCT and ICG images were obtained. However, use of the same source for OCT and fluorescence excitation could become increasingly difficult as either the source bandwidth increases or fluorophore emission intensity decreases, unless very large Stoke's shift NIR-excitable agents become available.

A strategy to provide greater spectral separation has been described [84]. This custom system included a mode-locked Ti:Sapphire laser and a 0.9 numerical aperture water immersion objective to generate simultaneous *en*

Fig. 26.2. (Continued) Extinction of gold nanoshells on a 60nm silica core are illustrated as a potential OCT scattering contrast agent [82]. *Bottom panel*: Emission of collagen type I gel and an epithelial cell suspension is shown at 280, 350 and 450 nm excitation. CyDye emission of Cy3 and Cy7 [141] are shown. Emission of clinically used fluorophores ICG [142], fluorescein (Molecular Probes/Invitrogen) and Protoporphyrin IX [141] are illustrated. Quantum dot emission from CdSe [139, 140] and InAs [139] are shown

face optical coherence and two-photon-excited fluorescence images. An image of a green fluorescent protein expressing drosophila embryo was presented; presumably endogenous fluorophore distribution could be imaged as well. Because fluorescence occurred at a much shorter wavelength range, no difficulties were encountered separating the fluorescence from the backscattered light. However, implementation of this method in an endoscopic fashion would be technically challenging because of high peak-power needs, three-dimensional scanning requirements, and need to control probe-tissue separation.

26.5.4 Materials

As described above, interesting endogenous fluorophores are best excited at ultraviolet wavelengths that also cause autofluorescence in most optical materials. Many glasses and polymers exhibit autofluorescence that is similar in spectral shape and range to the fluorescence of endogenous tissue fluorophores [85]. Because probe autofluorescence can easily become significant compared to the tissue signal, each component of the OCT-LIF system should be considered for autofluorescence, particularly if the excitation wavelength lies in the UV. The location of the element within the system is equally important as the absorption and emission characteristics of the material. Autofluorescence from an optically thick piece of fiber is generally more significant than from the same material used in a thin window. Additionally, isotropically emitted fluorescence is more easily collected from an element located near focus than from a lens or window located far from focus or in a low numerical aperture portion of the beam path. Lenses and windows made of fused silica and CaF_2 have low fluorescence under UV excitation, good NIR transmission, and are recommended throughout the beam path. Thick windows near the tissue should be restricted to lowest fluorescence glasses, although very thin windows of other glasses and even some low fluorescence plastic films may be acceptable [86]. Usually, some fluorescent materials must be used despite the best attempts to avoid them. For example, the emission from even "low fluorescence" ultraviolet transmitting optical epoxies is significant and care should be taken to keep glue joints thin [87]. The jacketing materials available on many commercially available communications grade fibers ideal for OCT fluoresce strongly. Although fiber choice could be restricted only to low fluorescence jacketed materials, it is often more practical to simply shield the fiber from UV excitation. This approach of hiding the fluorescent material behind absorbent material, a dichroic filter, or simply out of the beam path is the most flexible and commonly used. Care should be taken with items outside the device that may also autofluoresce, including tissue index matching gels, preservation media, culture plates, or wax mounting blocks.

26.5.5 Safety

The tip of a combined LIF/OCT endoscope is either in contact with or at a close distance to a tissue surface or body fluid, and therefore should be

analyzed for potential hazards. A thorough analysis of potential risks and protection against those risks is a requirement for human subject studies. Hazards include electrical shock hazards, clinical hazards, material toxicity hazards, and radiation hazards. Of unique importance to combined OCT/LIF systems is the fact that both systems may be operated concurrently, requiring cumulative radiation exposure analyses. Radiation exposure in the UV poses a different hazard than in the visible/NIR. UV exposure is a cumulative hazard (exposure limits can be calculated for repeated exposure over days) and visible and NIR light exposure is analyzed for potential thermal injuries. Threshold limit values for radiation exposure are defined by several standardization organizations: The American National Standards Institute (ANSI) publishes maximal permissible exposure levels [88]; the American Conference of Governmental Industrial Hygienists (ACGIH) publishes similar threshold limit values (TLV) and biological exposure indices [89]. In contrast to the above listed standardization organizations, the International Commission on Non-ionizing Radiation Protection (Oberschleissheim, Germany) makes their guidelines available online at no cost and publishes them in Health Physics. Usually the threshold limit values are expressed for laser beam [90, 91] and incoherent exposure [92, 93] of the eye and skin. For broadband UV exposure (<400 nm), the biologically effective radiation (device emission weighted by the biologic action spectrum, which is normalized at 270 nm) should not exceed the TLV for melano-compromised skin and eye ($3\,\mathrm{mJ/cm^2}$) [92]. The TLV for skin and eye has also been recommended for the cervix in a guidance document developed by the US Food and Drug Administration's center for device and radiological health (CDRH) [94]. For the wavelength range of 0.38 to μm, exposure limits are governed by thermal injury to the skin and eye. Unfortunately, the authors are not aware of any studies evaluating combinational effects of NIR radiation and UV exposure.

26.5.6 Optical Design Considerations

The optical design of a combined system is result of an attempt to optimally control the photon paths in the tissue for each modality, while meeting material constraints in the optical path, and separating the signals (chromatically, spatially, or temporally) to the appropriate detector. The useful signal in OCT depends on photons that undergo a single scattering event in a nearly backscattering direction. The confocal design of typical OCT systems helps reject photons that take any other path. Lateral resolution is dependent upon the beam cross section at a given depth. Usually, a balance between lateral resolution and depth of focus is struck in order to avoid axially scanning the objective [95]. Conversely, LIF photons are typically allowed to take a circuitous path: The excitation light may be scattered multiple times before it is absorbed. If fluorescence conversion occurs, the emission spectrum of the intrinsic fluorescence will be modified as the emitted photons wander randomly through the tissue until they are absorbed by chromophores or released

at the tissue surface. The path taken, and volume subsequently probed by the LIF system depends on the tissue absorption and scattering properties, as well as factors determined by the probe geometry: the insertion angles of excitation photons, the distance along the surface to the collection point (Source Detector Separation Distance – SDSD), and the angles over which the photons are collected. Fiberoptic probes have been proposed for preferential depth sensitive fluorescence sensing with the use of variable illumination and collection apertures [96, 97], illumination collection distances [97–100] and illumination collection angles [101–103].

Monte Carlo analysis of specific fiber optic probe implementations on media with tissue-like optical properties and their associated experimental verifications show trends that are useful in designing an LIF probe. First, it is critical to control the distance between the illumination/collection fibers and the tissue for quantitative tissue analysis [104,105]. When the illumination and collection areas are superimposed at the tissue surface (SDSD = 0), either by means of single illumination-collection fiber in contact with the tissue, or a spacer distal to a group of fibers that allows the illumination-collection areas to diverge over the same tissue area, the probe will be primarily sensitive to superficial layers less than 400 μm deep [104, 106, 107]. Similarly shallow tissue sampling can be achieved when source and collection fibers are separated at the tissue surface, but are inclined towards each other to cause an overlap of the fiber numerical apertures in the superficial tissue [108–110]. The average probed depth can be increased from 700 to 1200 μm by placing normally incident illumination and collection fibers that are directly in contact with the tissue at increased separation [104, 106, 107]. Evidence with diffuse reflectance modeling suggests that the probed depth can be increased yet further by inclining the fibers away from each other [111]. In general, greater overlap of the numerical apertures of the illumination and collection fibers improves collection efficiency while the expected probing depth decreases. The lateral extent of a collected LIF photon's path has been relatively unexplored, although lateral resolution somewhat larger than the SDSD could be expected. Increasing the fiber core diameter and numerical aperture increase the light gathering capacity of the collection fiber, but may have effects on the depth of collected fluorescence that depend upon the configuration. In cases with fibers in contact with the tissue, the size of the illumination and collection area introduces a superposition of many SDSDs, while the numerical aperture of the fiber introduces a superposition of many angles of insertion and collection. In addition to the depth selectivity provided by SDSD, some geometries appear to be optimally sensitive to fluorophore distribution rather than scattering properties of the tissue [112, 113]. Knowledge of tissue layer thicknesses from OCT images could help in the selection of optimal LIF illumination/detection fiber configurations.

26.6 Combined OCT/LIF System Examples

Of many potential implementation, three designs are discussed below: a free-space system, an endoscopic LIF image-guided OCT probe, and an endoscopic OCT/scanning-point LIF system. The free space system is conceptually simple and introduces several system design elements. However, combined OCT-LIF endoscopes are potentially more useful because they allow examination of a variety of mucosal tissues *in situ*. Clinically it is interesting to have tools that can monitor disease non-invasively or to guide traditional biopsy techniques. Because tissue degrades structurally and biochemically with time after excision, *in vivo* endoscopic studies potentially have the most accurate and conclusive diagnostic capability. At the same time, the small packages and biocompatibility requirements of endoscopes present a challenge to the designer. The two very different combined OCT-LIF endoscopes presented here embody the design principles discussed in the previous section. At the end of this section we describe some interesting challenges for OCT-LIF endoscopes and speculate on how these challenges might be addressed.

26.6.1 Combined OCT-LIF System with Free-Space Sample Arm Example

Spectral separation is used to isolate the signals in our first example: a benchtop device used to collect simultaneous OCT-LIF data from *ex vivo* tissues [114]. A fiber-based time domain OCT system is mated to a free space LIF system by combining the beams for each system at a dichroic beamsplitter located shortly before the final focusing objective. The long pass filter mirror transmits the near-IR OCT beam ($\lambda_o = 1300\,\text{nm}$ $\Delta\lambda = 49\,\text{nm}$) while reflecting the excitation wavelength (325 or 442 nm) and the emission spectrum (350–700 or 460–700 nm). A sharp edge filter is used in the LIF system to separate the excitation line from the emission spectrum before entrance into the spectrometer optics. When the OCT beam is focused to a depth of 300 µm, chromatic aberration in the CaF_2 objective causes the LIF excitation beam to be focused 2.4 mm above the tissue resulting in a 70 µm illumination area at the tissue surface. The emission from this area is imaged onto a CCD spectrometer. A block diagram of the system is given in Fig. 26.3.

In this configuration, the beamsplitters and the final objective lens present the largest autofluorescence risk, while the majority of the OCT system never sees any significant scatter from the excitation laser or the emitted fluorescence (which could cause increase shot noise if not filtered prior to the OCT detector). The wavelength of the OCT beam is beyond the response range of the spectrometer. Because the illumination-collection areas are superimposed and small, this system is primarily sensitive to superficial fluorophores. Though the non-contact approach of the LIF portion of this device does not constrain the illumination-collection geometry, distance information contained in the

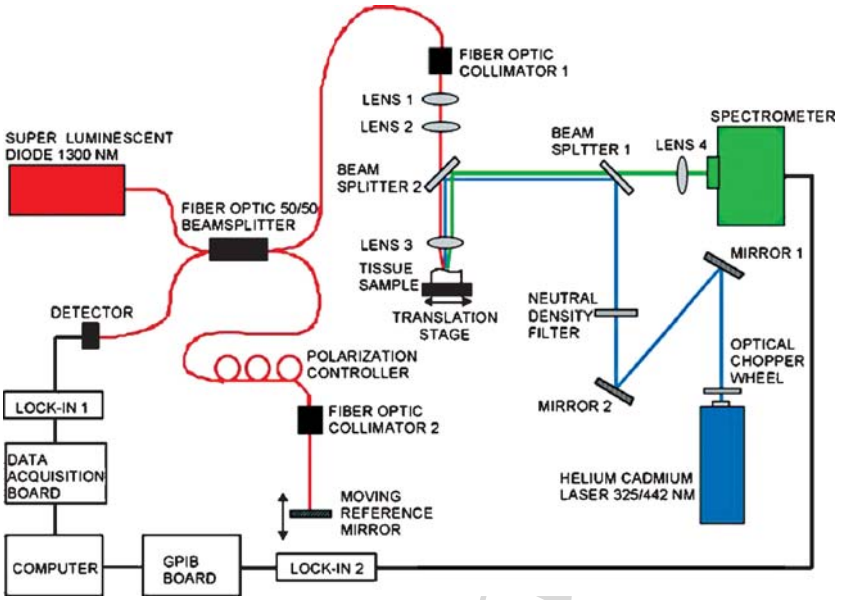

Fig. 26.3. Free space combined OCT/LIF system. The red, blue, and green lines represent the optical paths of the OCT, excitation, and emission light, respectively. Adapted from [114]

optical coherence tomogram could be used to correct the resulting variation in spectra, as described earlier.

This device has been used to investigate a variety of *ex vivo* samples. In one study with autopsy aorta specimens [114], data from each modality corresponded closely with results from previous research. Optical coherence tomograms showed layered features associated with the intima, media, and internal elastic lamina in normal aorta, and dissections, lipid pools, and fibrosis in areas of atherosclerotic plaque. Simple threshold based analysis on LIF emission spectra ratios 520/490 nm (325 nm excitation) and 595/635 nm (442 nm excitation) were used to identify normal and plaque regions with 97 and 91% correct classification rate respectively.

26.6.2 LIF Guided OCT Endoscope

McNichols et al. [78] developed a 1.5 cm diameter rigid endoscopic probe with a superimposed fluorescence imaging field and an OCT line scan [115]. The probe was constructed by combining a rigid imaging endoscope with an end-scanning endoscopic OCT probe ($\lambda_o = 1300$ nm) at a dichroic beamsplitter. A filtered xenon arc lamp (410 nm) was coupled into a fiber ring illuminator to deliver excitation light to the tissue. A 650 nm broadband filter was used to isolate the emission before measurement by a CCD video camera. A dia-

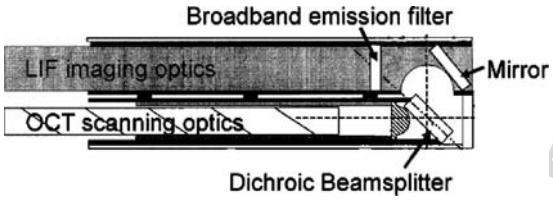

Fig. 26.4. Diagram of the distal tip of a combined OCT/LIF imaging system. From US patent 6,507,747 Gowda et al.

gram of the distal tip of this device is shown in Fig. 26.4. This device used autofluorescence imaging as a sensitive method to rapidly identify suspicious regions on carcinogen-treated everted hamster cheek pouches, for subsequent inspection with OCT to obtain a more specific morphological diagnosis. In testing, OCT was able to confirm atypia as well identify false positive areas identified by fluorescence imaging.

Like the "benchtop" system described above, chromatic separation is used to isolate the OCT-LIF signals. Filters placed close to the sample isolate the imaging optics and prevent them from being an autofluorescence risk. Uniformly illuminating the field of view and imaging the emitted light is likely to be primarily sensitive to superficial fluorophores because of the greater efficiency of exciting superficial layers, although photon paths do exist with a large SDSD. Although this system is not intended for detailed spectroscopic analysis of the fluorescent image, variable illumination-collection geometry over the field of view could be compensated by normalization with reflectance data.

26.6.3 OCT/Scanning-point LIF Endoscope

Spatial and spectral signal separation is used in our third example of a dual modality device. In this case, OCT and LIF channels run in parallel fibers down to the tip of an endoscopic probe. The OCT channel is focused in the tissue by a GRIN lens while the LIF channel bypasses the GRIN and fires directly on the tissue, unlensed. Two multimode fibers located on either side of the excitation fiber sample the emitted light and carry it back to a spectrometer. The scanning action of the endoscope causes the OCT beam to cross the same section of tissue moments after the LIF system has collected spectra there. Post processing software correlates the two scans [116].

This system stays close to a very traditional OCT endoscope design while using the window in contact with the tissue to maintain a fixed illumination-collection geometry for LIF. A block diagram of the combined OCT/LIF system is shown in Fig. 26.5, and details of the endoscope in Fig. 26.6. The 2.4 mm pathlength between the LIF fibers and the tissue allows the illumination-collection areas to expand to an overlapping 1.25 mm spot yielding sensitivity primarily to superficial layers. The large spot yields relatively

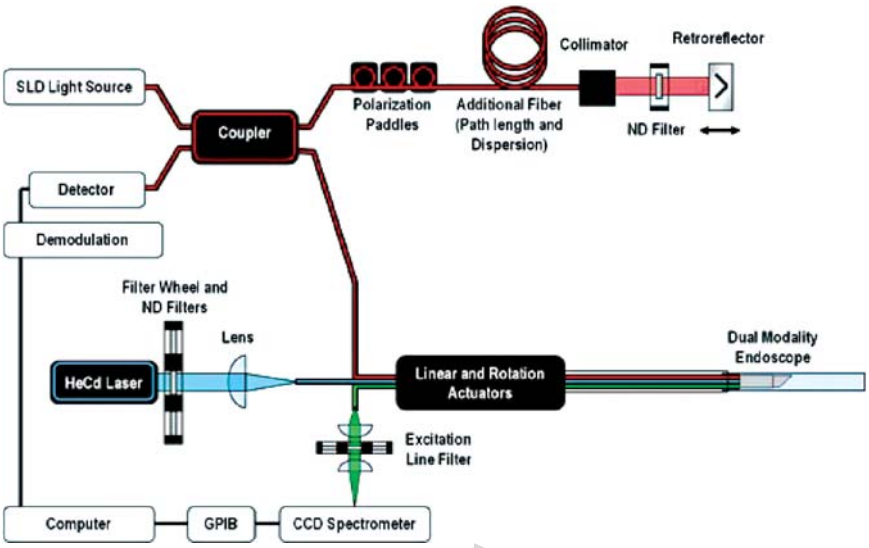

Fig. 26.5. A block diagram of the OCT/scanning-point LIF endoscopic system shows how the two subsystems meet at the endoscope tip and at the data acquisition computer. CCD: charge coupled device, GPIB: general purpose interface bus, HeCd: Helium:Cadmium, ND: neutral density filter, SLD: superluminescent diode

low transverse LIF resolution. Separate illumination and collection fibers are used which minimizes collection of specular backreflection and autofluorescence from within the excitation fiber. By bypassing the GRIN lens, it is possible to achieve low collected autofluorescence, even though the GRIN material used to focus the OCT beam is highly fluorescent. No direct path exists to excite the GRIN material or to collect that fluorescence. Diffusely reflected excitation light must be absorbed by the GRIN lens, be emitted back in the direction of the tissue and be further diffusely reflected back into the collection fiber, an improbable occurrence. Other considerations taken to reduce the autofluorescence potential of the probe were a fused silica window, aluminum jacketed multimode fibers, low fluorescence optical cement, and shielding the circumference of the GRIN lens with black permanent marker. This probe has been successfully applied to several tissues, two of which are described at the end of this chapter.

26.6.4 Alternative Endoscope Designs

Dual-modality endoscopic designs can be modified to address opportunities that have been identified by recent research in each field. As center wavelengths shorten and bandwidths increase for ultrahigh axial resolution OCT, there is increased risk of overlap with the endogenous and exogenous fluorophore emission spectra. The loss of spectral separation forces

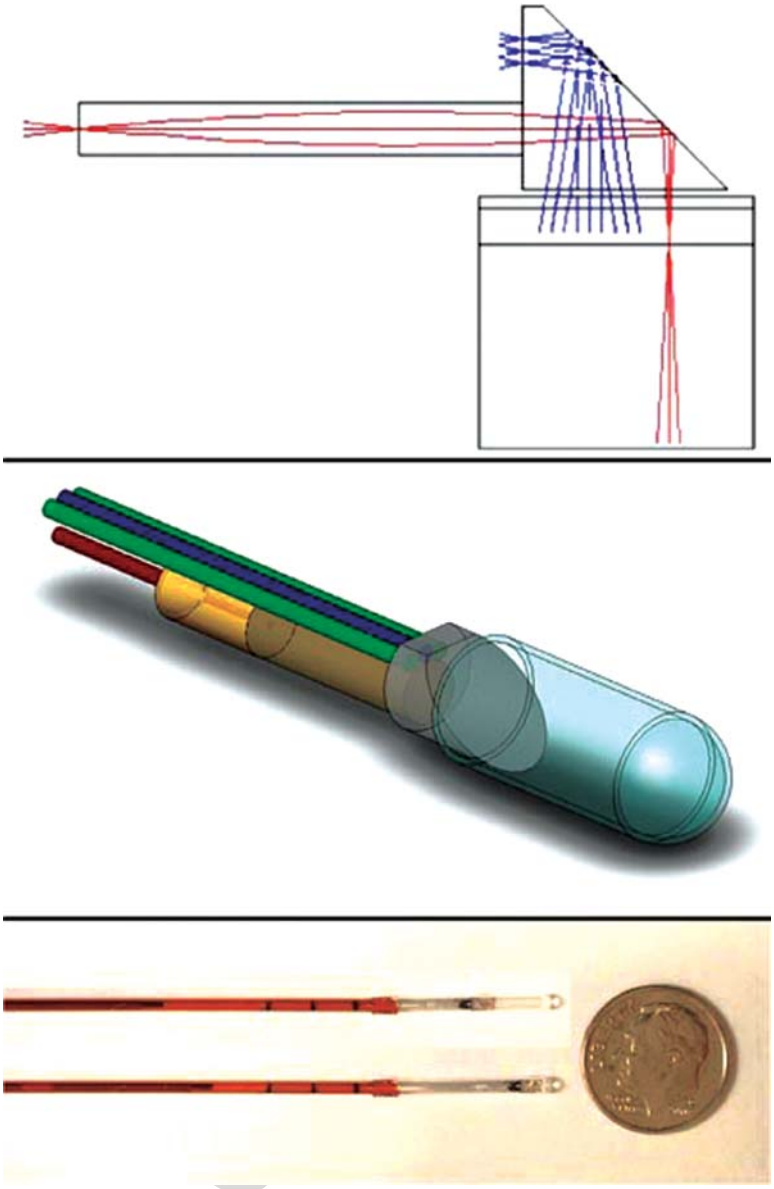

Fig. 26.6. Details of the combined OCT/LIF scanning-point endoscope. *Top*: optical raytrace with OCT path in red and LIF excitation/emission in blue. *Middle*: solid rendering with OCT optical fiber in red, LIF excitation fiber in blue, LIF emission collection fibers in green, ferrule, GRIN lens, and rod prism in yellow, and glass envelope in blue. *Bottom*: Photograph of the endoscope with the tip translated to two different positions. Adapted from [116]

a move towards spatial or temporal separation. The limited selection of low-fluorescence glasses also reduces a lens designers options when attempting to control chromatic and pupil aberrations. It is also interesting to provide improved depth specificity by better control of the SDSD or the insertion-collection angles. One alternative endoscope design is shown in Fig. 26.7 top panel. Side-firing LIF fibers are aimed out of the endoscope 180° offset from the OCT beam. If the endoscope is precisely rotated, then well-aligned (albeit not quite simultaneously collected) OCT-LIF scans result. This serves to increase the OCT-LIF spatial separation, which mitigates problems

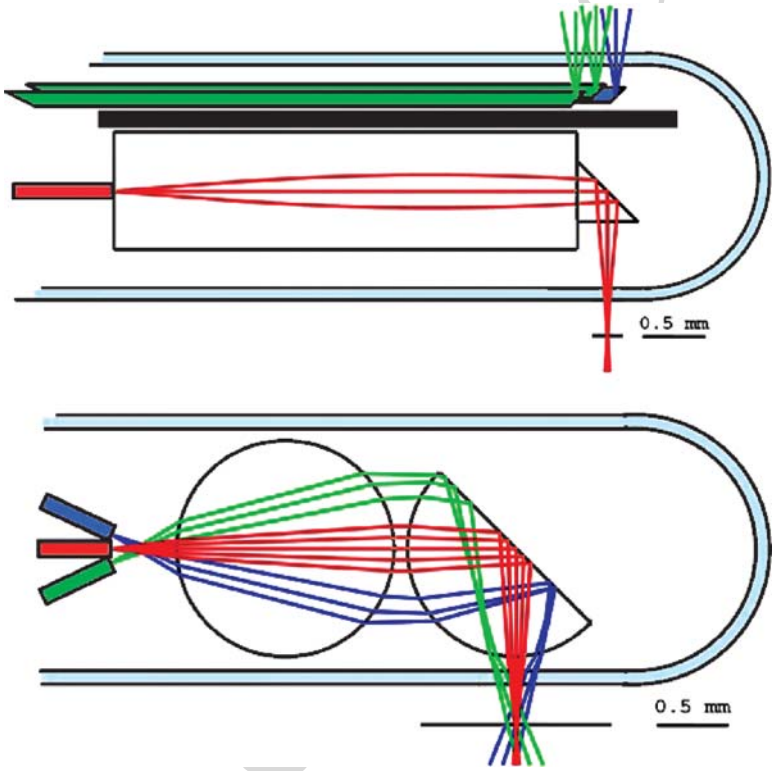

Fig. 26.7. Potential designs for OCT/LIF endoscopes. *Top*: LIF channels fire in opposite direction from the OCT channel (red) to maximize spatial separation. Multiple collection fibers (green) placed at increasing SDSD from the illumination fiber (blue) allow for specificity to multiple depths. A barrier (heavy black) placed behind the LIF fibers prevents collection of autofluorescence from the GRIN lens. *Bottom*: a pair of fused silica ball lenses provides diffraction limited performance for an on-axis OCT channel (red) and overlaps LIF illumination (blue) and collection (green) channels at a depth 0.3 mm into tissue. Note that all channels are shown in a single sagittal plane for illustration only; out of plane construction allows better use of the lens aperture and may allow for more and larger collection fibers

of autofluorescence and spectral overlap between OCT and LIF. By placing the fiber apertures nearer the tissue, the resolution and potential efficiency of LIF path is increased. If multiple collection fibers are placed with different SDSDs, specificity to multiple depths can be achieved. In another alternative design, the GRIN lens is replaced with traditional microoptics made in low fluorescent glass (Fig. 26.7 bottom panel). This allows the fibers of the LIF portion of the instrument to be imaged into the tissue in the same path as the OCT. Imaging the LIF fibers into the tissue improves resolution and potential collection efficiency similarly to placing the fibers nearer to the tissue. Depth sensitivity might be achieved by overlap of the illumination-collection areas at a targeted tissue depth. One low cost lens design that provides low fluorescence and diffraction limited on axis performance for OCT is a pair of ball lenses.

26.7 Example Applications

To conclude this chapter, we describe two applications of the combined OCT/scanning-point LIF endoscope described earlier: *in vivo* imaging of mouse colon and *ex vivo* imaging of rat ovary. Both applications demonstrate the successful simultaneous acquisition of OCT images and LIF spectra, and provide evidence that the data types are complimentary.

26.7.1 Mouse Colon

The OCT/LIF endoscope provides access to the distal 3 cm of the mouse colon. *In vivo* monitoring in a mouse model may enable extrapolation about the capability of OCT-LIF to identify cancer in a human patient, as well as aid in the development of mouse colon disease models. The normal mouse colon is approximately 300 µm thick with an average crypt measuring 100 by 20 µm. Epithelial cancers start as aberrant crypt foci (ACF) that are little larger than a collection of several crypts, and may become large adenomas over 1mm in diameter. In the digestive tract, chromophores common to other tissues (including collagen, NADH, and hemoglobin) are present in combination with those found in the digested food.

OCT-LIF data have been collected in anesthetized tumor model ($APC^{min/+}$) mice using linear scans along the distal 3 cm of colon at 8 rotations, providing sufficient coverage to observe large amounts of normal tissue and to ensure that no large adenoma is undetected. In a study observing these tumor model mice over a period of 16 weeks, Hariri et al. found that in regions of histologically identifiable adenoma, OCT first showed mucosal thickening and then development of an abnormal mass with loss of layered structure. Corresponding spectra showed significantly higher 680 nm emission relative to 405 nm emission at the sight of adenoma [117].

McNally et al. [118] used this instrument just prior to sacrifice of tumor model mice ($APC^{min/+}$) to compare OCT-LIF with laser scanning confocal fluorescence microscopy and traditional histology. In tumor regions identified by OCT and confirmed by histology, a drop in absolute signal at 390 nm and 450 nm were observed along with a rise at 680 nm. Using a simple test that required a drop below a threshold value at 390 and 450 nm as well as a rise above a threshold at 680 nm, McNally used the LIF data to detect adenoma with 81% sensitivity and 80% specificity. By varying the amount of chlorophyll in the diet of these mice, the investigators were able to confirm that the 680 nm fluorescent signal was in fact correlated with chlorophyll intake. *En face* laser scanning confocal fluorescence microscopy could identify individual fluorescing particles as fecal contamination at the surface of some adenoma but was unsuccessful at determining the distribution of a deeper, more diffuse source of red fluorescence in the tissue. An example OCT/LIF image pair taken from a mouse with a large adenoma is shown in Fig. 26.8. The adenoma is apparent both from the loss of normal layered structure in the OCT image, and the dramatic drop in fluorescence emission intensity in the 350–600 nm range with corresponding strong emission intensity at 680 nm. Figure 26.9 shows the mean and standard deviation of fluorescence emission ratios at

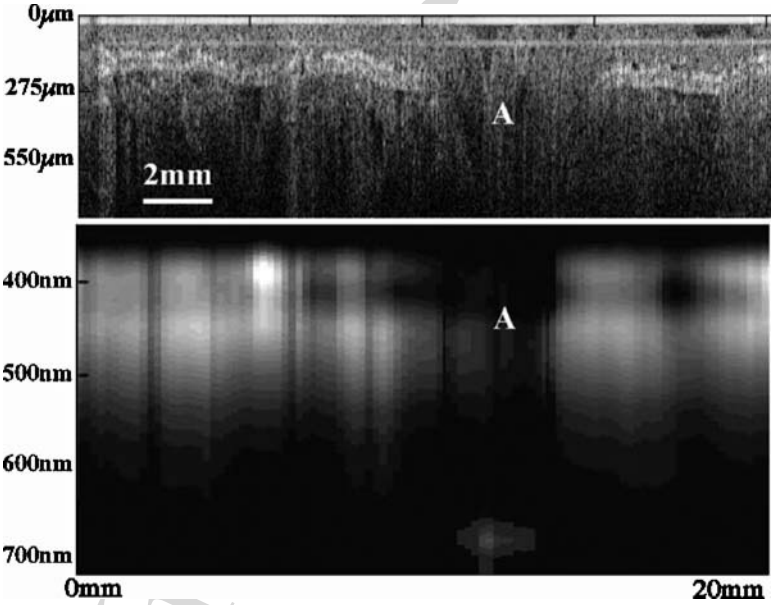

Fig. 26.8. OCT-LIF spectra of an adenoma in mouse colon. The adenoma can be visualized in the OCT image (*top*) as a loss of normal layered structure. The corresponding LIF signals (*bottom*) show a significant reduction in the 390 nm and 450 nm signal and a peak in the 680 nm signal over the adenomatous region. Figure reprinted from [118]

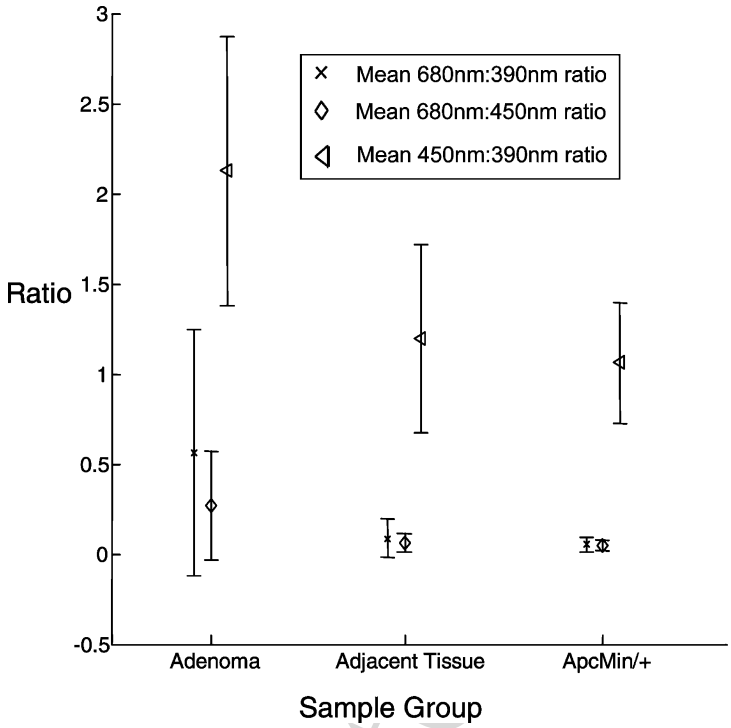

Fig. 26.9. Mean and standard deviation of 680:390 nm, 680:450 nm and 450:390 nm emission ratios (325 nm excitation) collected at the site of adenoma, tissue adjacent to adenoma, and undiseased colon in the same breed of mice. Adenoma show increases in all three ratios. Adapted from [118]

680:390 nm, 680:450 nm and 450:390 nm for adenoma, histologically normal tissue in adenomatous colons, and tissue from mice with no colonic adenomas.

OCT data so far have been used primarily to identify areas of the mouse colon that are abnormal and to use this data to isolate matching fluorescence spectra associated with tumors. Statistically significant differences between normal and tumor tissues have been observed in LIF spectra, but the variation in fluorescence signal in normal tissue limits sensitivity and specificity. It seems likely that details in the OCT image such as changes in mucosal layer thickness, or presence of adventitia surrounding the colon can be associated with fluctuations in the fluorescence spectra. This highlights the complementary, but non-orthogonal, nature of the datasets, and the potential to improve fluorescence diagnostics with knowledge of the underlying tissue structure.

26.7.2 Rat Ovary

A similar endoscopic combined OCT/LIF system was used to acquire images and spectra of 54 excised rat ovaries [119]. While this study was *ex vivo*,

the endoscope was used in preparation for future minimally invasive *in vivo* studies. The goal of this study was to determine if OCT and/or LIF could distinguish between ovaries from normal cycling animals, post-menopausal ovaries (follicle depletion induced by i.p. injection of 4-vinylcyclohexene diepoxide, or VCD), and ovaries with atypia or neoplasms induced by 7, 12—Dimethylbenz-alpha-anthracene (DMBA). VCD was administered for 20 days at a dose of 160 mg/kg i.p. Three to five months later, some animals had a DMBA soaked suture (approximately 110 μg DMBA) placed through the right ovary. One to 5 months after suture insertion, the animals were sacrificed and the ovaries excised. Excess fat and connective tissue was trimmed prior to imaging; no superficial blood contamination was apparent.

Figure 26.10 shows a sequence of OCT images/LIF spectra and histology from a normal cycling ovary, VCD treated follicle deplete ovary, a VCD/DMBA treated ovary with atypia (follicular remnant degeneration), and a VCD/DMBA treated ovary with neoplastic cysts. In the cycling ovary, antral follicles and the bursa are seen. The VCD treated ovary is much reduced in size, and only dense stroma with surface fat is seen, as would be expected in a follicle-deplete, post-menopausal ovary. Follicular remnant degeneration in the DMBA treated ovary manifests as a multitude of small hypointense regions, whereas the cancerous cysts are large hypointense regions. The OCT images show excellent correspondence to histology at the tissue architecture level. While the DMBA-treated ovaries clearly appeared abnormal, a determination of neoplasia could not be made since the markers of cancer (e.g. abnormally large or irregular nuclei) were not identifiable at the resolution of this OCT system. Therefore, it appears that OCT may be of use in identifying abnormal-appearing ovaries but by itself cannot make a determination of atypical changes or neoplasia. Molecularly targeted contrast agents (absorption or scattering) could be of use to increase OCT's sensitivity and specificity to cancer.

The LIF spectra show peaks at approximately 390 nm and 450 nm, and absorption at 420 nm, associated with collagen fluorescence, NADH florescence, and hemoglobin absorption, respectively. In the normal cyling ovary, the magnitude of the 450 nm peak is greater than the 390 nm peak, and the dip at 420 nm is well defined. This suggests that a relatively large amount of NADH and hemoglobin is present in the ovary. In contrast, LIF spectra from the follicle deplete ovary is dominated by the 390 nm peak, indicative of high relative collagen content and less metabolic activity. There is also a relatively small amount of vasculature as seen from the LIF spectra (less pronounced dip at 420 nm), which was confirmed histologically. The DMBA treated ovaries both show a relatively high 450 nm fluorescence peak and pronounced 420 nm absorption, similar to the cycling ovary. A comparison between groups shows statistically significant differences in the ratio of 390:450 nm fluorescence intensity of the cycling and cancerous groups, as compared to follicle deplete group.

In summary, the feasibility of using the combined OCT/LIF system to determine the presence of atypical and neoplastic changes in the ovary was

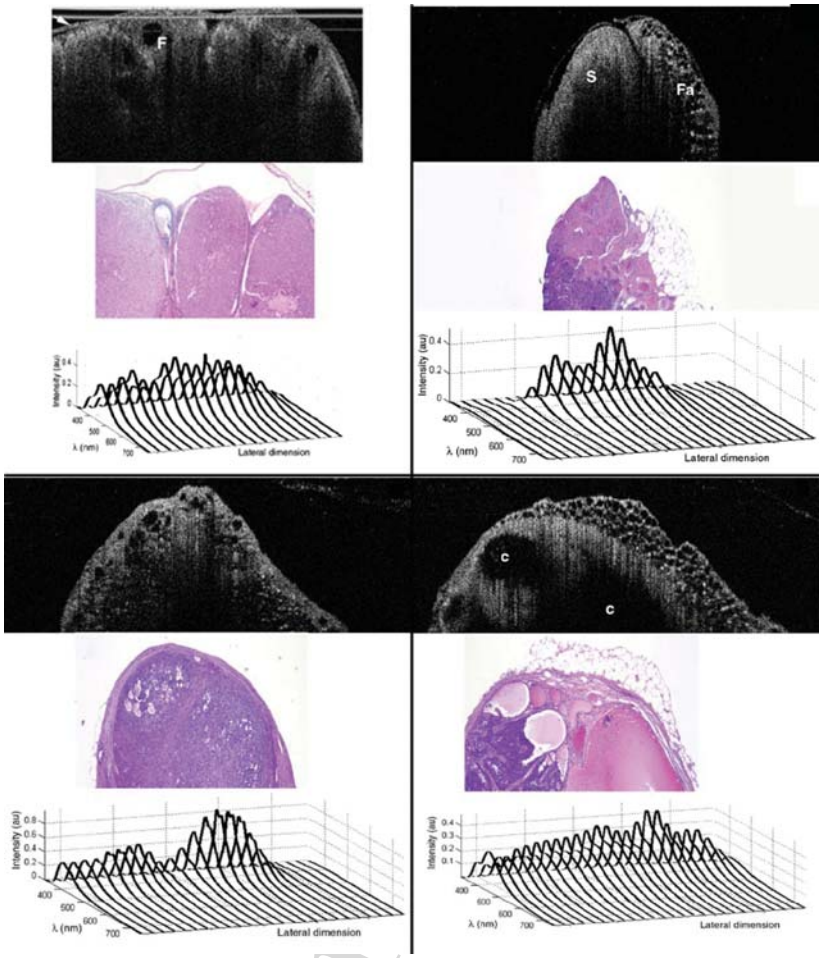

Fig. 26.10. A sequence of OCT images, LIF spectra, and histology from a normal cycling ovary (*top left*), VCD treated follicle deplete ovary (*top right*), a VCD/DMBA treated ovary with atypia- follicular remnant degeneration (*bottom left*), and a VCD/DMBA treated ovary with neoplastic cysts (*bottom right*). The normal cycling ovary shows follicular cysts (F), whereas the follicle deplete ovary has only dense stroma (S) and fat (Fa). Many small abnormal cysts are seen in the atypical ovary, and large abnormal cysts (C) are seen in the neoplastic ovary. OCT images correlate well with histology. LIF shows a trend towards increased 450:390 nm fluorescence emission ratio in metabolically active ovaries (either normal cycling or atypical/neoplastic) compared to the follicle deplete ovary. OCT images are 5 mm lateral × 1.4 mm deep, except normal cycling which is 4 mm lateral. Histology is to same scale as OCT. LIF data are presented over the same lateral range as the OCT images. Adapted from [119]

shown. Different structures such as cysts, fatty regions and follicular remnant degeneration were easily identified in the OCT images. There was preliminary evidence from this study that atypical cellular changes might be located in the regions identified by irregularly sized hypointense regions in the OCT images, but OCT could not directly distinguish atypical cells and areas of cancer. The LIF spectra provided information about hemoglobin content as well as the metabolic activity of the ovary, and displayed significant changes between follicle deplete emission ratios and both cycling and neoplastic emission ratios. Therefore, this study suggested that by utilizing combined OCT and LIF data, it may be possible to distinguish between cycling, follicle deplete, non-atypical, atypical and neoplastic ovaries.

26.8 Conclusion

In this chapter, existing combined OCT/LIF endoscopic systems were described, and potential improvements in resolution and collection efficiency with alternative optical designs were presented. There is evidence that the combination of OCT and LIF is synergistic in several respects. First OCT can provide information about subsurface structures that can aid interpretation of LIF spectra. Second, quantitative measures of tissue layer thickness and probe-tissue separation can be used in models that seek to extract intrinsic fluorescence or correct for tissue distance. Third, LIF imaging can be used as a guidance technique to direct OCT imaging to potentially diseased areas. Finally, if criteria are properly developed for both modalities, the combination of the two may increase sensitivity and/or specificity to disease. Future work will help define the applications most enhanced by this dual modality approach.

References

1. J. F. De-Boer, T. E. Milner, M. J. C. van-Gemert and J. S. Nelson, "Two-dimensional birefringence imaging in biological tissue by polarization-sensitive optical coherence tomography," Optics Letters. 22(12), 934–6 (1997).
2. G. Yao and L. V. Wang, "Two-dimensional depth-resolved Mueller matrix characterization of biological tissue by optical coherence tomography," Optics Letters. 24(8), 537–9 (1999).
3. C. K. Hitzenberger, E. Gotzinger, M. Sticker, M. Pircher and A. F. Fercher, "Measurement and imaging of birefringence and optic axis orientation by phase resolved polarization sensitive optical coherence tomography," Optics Express. 9(13), (2001).
4. J. F. de Boer and T. E. Milner, "Review of polarization sensitive optical coherence tomography and Stokes vector determination," J Biomed Opt. 7(3), 359–71 (2002).

5. J. Zang, S. Guo, W. Jung, J. S. Nelson and Z. Chen, "Determination of birefringence and absolute optic axis orientation using polarization-sensitive optical coherence tomography with PM fibers," Optics Express. 11(24), (2003).
6. Z. Chen, T. E. Milner, D. Dave and J. S. Nelson, "Optical Doppler tomographic imaging of fluid flow velocity in highly scattering media," Optics Letters 22(1), 64–66 (1997).
7. J. A. Izatt, M. D. Kulkarni, S. Yazdanfar, J. K. Barton and A. J. Welch, "In vivo bidirectional color Doppler flow imaging of picoliter blood volumes using optical coherence tomography," Optics Letters 22(18), 1439–1441 (1997).
8. V. X. D. Yang, M. L. Gordon, Bling-Qi, J. Pekar, S. Lo, E. Seng-Yue, A. Mok, B. C. Wilson and I. A. Vitkin, "High speed, wide velocity dynamic range Doppler optical coherence tomography (Part I): System design, signal processing, and performance," Optics Express 11(7), (2003).
9. R. A. Leitgeb, L. Schmetterer, W. Drexler, A. F. Fercher, R. J. Zawadzki and T. Bajraszewski, "Real-time assessment of retinal blood flow with ultrafast acquisition by color Doppler Fourier domain optical coherence tomography," Optics Express 11(23), (2003).
10. M. Sticker, C. K. Hitzenberger, R. Leitgeb and A. F. Fercher, "Quantitative differential phase measurement and imaging in transparent and turbid media by optical coherence tomography," Optics Letters 26(8), 518–20 (2001).
11. C. G. Rylander, D. P. Akkin, T. E. Milner, K. R. Diller and A. J. Welch, "Quantitative phase-contrast imaging of cells with phase-sensitive optical coherence microscopy," Optics Letters 29(13), 1509–11 (2004).
12. C. Joo, T. Akkin, B. Cense, B. H. Park and J. F. de-Boer, "Spectral-domain optical coherence phase microscopy for quantitative phase-contrast imaging," Optics Letters 30(16), 2131–3 (2005).
13. C. Yang, "Molecular contrast optical coherence tomography: a review," Photochem. Photobiol. 81(2), 215–237 (2005).
14. S. A. Boppart, A. L. Oldenburg, Chenyang-Xu and D. L. Marks, "Optical probes and techniques for molecular contrast enhancement in coherence imaging," Journal of Biomedical Optics 10(4), 41208–14 (2005).
15. U. Morgner, W. Drexler, F. X. Kartner, X. D. Li, C. Pitris, E. P. Ippen and J. G. Fujimoto, "Spectroscopic optical coherence tomography," Optics Letters 25, 111–113 (2003).
16. K. D. Rao, M. A. Choma, S. Yazdanfar, A. M. Rollins and J. A. Izatt, "Molecular contrast in optical coherence tomography by use of a pump-probe technique," Optics Letters 28(5), 340–2 (2003).
17. J. S. Bredfeldt, C. Vinegoni, D. L. Marks and S. A. Boppart, "Molecularly sensitive optical coherence tomography," Optics Letters 30(5), 495–7 (1977).
18. Y. Jiang, I. Tomov, Y. Wang and Z. Chen, "Second-harmonic optical coherence tomography," Optics Letters 29(10), 1090–2 (2004).
19. M. V. Sarunic, B. E. Applegate and J. A. Izatt, "Spectral domain second-harmonic optical coherence tomography," Optics Letters 30(18), 2391–3 (2005).
20. J. K. Barton, J. B. Hoying and C. J. Sullivan, "Use of Microbubbles as an Optical Coherence Tomography Contrast Agent," Acad. Radiol. 9(S1), S52–S55 (2002).
21. T. M. Lee, A. L. Oldenburg, S. Sitafalwalla, D. L. Marks, W. Luo, F. J. Toublan, K. S. Suslick and S. A. Boppart, "Engineered microsphere contrast agents for optical coherence tomography," Optics Letters 28, 1546–1548 (2003).

22. C. Loo, A. Lin, M. Lee, J. K. Barton, N. Halas, J. West and R. Drezek, "Nanoshell-enabled photonics-based imaging and therapy of cancer," Technology in Cancer Research and Treatment 3, 33–40 (2004).
23. H. Cang, T. Sun, Z. Y. Li, J. Chen, B. J. Wiley, Y. Xia and X. Li, "Gold nanocages as contrast agents for spectroscopic optical coherence tomography," Optics Letters 30(22), 3048–50 (2005).
24. G. Isenburg, M. V. Sivak, A. Chak, R. C. Wong, J. E. Willis, B. Wolf, D. Y. Rowland, A. Das and A. Rollins, "Accuracy of endoscopic optical coherence tomography in the detection of dysplasia in Barrett's esophagus: a prospective, double-blinded study," Gastrointest Endosc. 62(6), 825–831 (2005).
25. M. J. Manyak, N. D. Gladkova, J. H. Makari, A. M. Schwartz, E. V. Zagaynova, J. M. Zara, R. Iksanov and F. I. Feldchtein, "Evaluation of superficial bladder transitional-cell carcinoma by optical coherence tomography," J Endourol. 19(5), 570–4 (2005).
26. H. Yabushita, B. E. Bouma, S. L. Houser, H. T. Aretz, I. K. Jang, K. H. Schlendorf, C. R. Kauffman, M. Shishkov, D. H. Kang, E. F. Halpern and G. J. Tearney, "Characterization of human atherosclerosis by optical coherence tomography," Circulation 106(13), 1640–5 (2002).
27. B. Shen, G. Zuccaro, T. L. Gramlich, N. Gladkova, P. Trillo, M. Kareta, C. P. Delaney, J. T. Conner, B. A. Lashner, C. L. Bevins, F. Feldchtein, F. H. Remzi, M. L. Bambrick and V. W. Fazio, "In vivo colonoscopic optical coherence tomography for transmural inflammation in inflammatory bowel disease," Clin Gastroenterol Hepatol. 2(12), 1080–7 (2004).
28. P. A. Testoni, B. Mangiavillano, L. Albarello, P. G. Arcidiacono, A. Mariani, E. Masci and C. Doglioni, "Optical coherence tomography to detect epithelial lesions of the main pancreatic duct: an Ex Vivo study," Am J Gastroenterol. 100(12), 2777–83 (2005).
29. J. R. Lakowicz. Principles of fluorescence spectroscopy, Kluwer Academic/ Plenum, New York, 1999.
30. G. A. Wagnieres, W. M. Star, and B. C. Wilson, "In vivo fluorescence spectroscopy and imaging for oncological applications," Photochem. Photobiol. 68, 603–632 (1998).
31. M. A. Mycek and B. W. Pogue. Handbook of biomedical fluorescence, Marcel Dekker, New York, 2003.
32. R. Richards-Kortum and Sevick-Muraca, "Quantitative optical spectroscopy for tissue diagnosis," Annu. Rev. Phys. Chem. 47, 555–606 (1996).
33. N. Ramanujam, "Fluorescence spectroscopy of neoplastic and non-neoplastic tissues," Neoplasia 2, 89–117 (2000).
34. K. Sokolov, M. Follen and R. Richards-Kortum, "Optical spectroscopy for detection of neoplasia," Curr. Opin. Chem. Biol. 6, 651–658 (2002).
35. T. Vo-Dinh. Biomedical photonics handbook, CRC Press, Boca Raton, Fla., 2003.
36. T. Galeotti, G. D. V. van Rossum, D. H. Mayer, and B. Chance, "On the fluorescence of NAD(P)H in whole-cell preparation of tumors and normal tissues," Eur. J. Biochem. 17, 485–49 (1970).
37. B. Chance, "Optical method," Annu. Rev. Biophys. Biophys. Chem. 20, 1–28 (1991).
38. B. Thorell and B. Chance, "Localization and kinetics of reduced pyridine nucleotide in living cells by microfluorometry," J. Biol. Chem. 234, 3044–3050 (1959).

39. Policard, "A study on the available aspects of experimental tumours examined by Wood's light," C. R. Seances Soc. Biol. Fil. 91, 1423–1424 (1924).
40. F. N. Ghadially, and W. J. Neish, "Porphyrin fluorescence of experimentally produced squamous cell carcinoma," Nature 188, 1124 (1960).
41. F. N. Ghadially, "Red Fluorescence of Experimentally Induced and Human Tumours," J. Pathol. Bacteriol. 80, 345 (1960).
42. K. T. Schomacker, J. K. Frisoli, C. Compton, T. J. Flotte, J. M. Richter, N. Nishioka, and T. F. Deutsch, "Ultraviolet Laser-Induced Fluorescence of Colonic Tissue: Basic Biology and Diagnostic Potential," Las. Surg. Med. 12, 63–78 (1992).
43. K. D. Ashby, J. Wen, P. Chowdhury, T. A. Casey, M. A. Rasmussen, and J. W. Petrich, "Fluorescence of dietary porphyrins as a basis for real-time detection of fecal contamination on meat," J. Agric. Food Chem. 51, 3502–3507 (2003).
44. L. F. Ma and D. Dolphin, "The metabolites of dietary chlorophylls," Phytochemistry 50, 195–202 (1999).
45. M. B. Ericson, J. Uhre, C. Strandeberg, B. Stenquist, O. Larko, A. M. Wennberg, and A. Rosen, "Bispectral fluorescence imaging combined with texture analysis and linear discrimination for correlation with histopathologic extent of basal cell carcinoma," Journal of Biomedical Optics 10, 034009 (2005).
46. S. Andersson-Engels, G. Canti, R. Cubeddu, C. Eker, C. af Klinteberg, A. Pifferi, K. Svanberg, S. Svanberg, P. Taroni, G. Valentini, and I. Wang, "Preliminary evaluation of two fluorescence imaging methods for the detection and the delineation of basal cell carcinomas of the skin," Lasers in Surgery & Medicine 26, 76–82 (2000).
47. E. Endlicher, P. Rummele, F. Hausmann, H. C. Rath, R. Knuchel, R. C. Krieg, J. Scholmerich, and H. Messmann, "Detection of dysplastic lesions by fluorescence in a model of chronic colitis in rats after local application of 5-aminolevulinic acid and its esterified derivatives," Photochemistry and Photobiology 79, 189–192 (2004).
48. J. Gahlen, J. Stern, J. Pressmar, J. Bohm, R. Holle, and C. Herfarth, "Local 5-aminolevulinic acid application for laser light-induced fluorescence diagnosis of early staged colon cancer in rats," Lasers in Surgery & Medicine 26, 302–307 (2000).
49. C. Eker, S. Montan, E. Jaramillo, K. Koizumi, C. Rubio, S. Andersson-Engels, K. Svanberg, S. Svanberg, and P. Slezak, "Clinical spectral characterisation of colonic mucosal lesions using autofluorescence and delta aminolevulinic acid sensitisation," Gut 44, 511–518 (1999).
50. M. Csanady, J. G. Kiss, L. Ivan, J. Jori, and J. Czigner, "ALA (5-aminolevulinic acid)-induced protoporphyrin IX fluorescence in the endoscopic diagnostic and control of pharyngo-laryngeal cancer," European Archives of Oto-Rhino-Laryngology 261, 262–266 (2004).
51. Y. T. Pan, T. Q. Xie, C. W. Du, S. Bastacky, S. Meyers, and M. L. Zeidel, "Enhancing early bladder cancer detection with fluorescence-guided endoscopic optical coherence tomography," Optics Letters 28, 2485–2487 (2003).
52. M. Olivo, W. Lau, V. Manivasager, T. P. Hoon, and C. Christopher, "Fluorescence confocal microscopy and image analysis of bladder cancer using 5-aminolevulinic acid," International Journal of Oncology 22, 523–528 (2003).
53. V. Manivasager, P. W. Heng, J. Hao, W. Zheng, K. C. Soo, and M. Olivo, "A study of 5-aminolevulinic acid and its methyl ester used in in vitro and in

vivo systems of human bladder cancer," International Journal of Oncology 22, 313–318 (2003).
54. R. M. Lycette, and R. B. Leslie, "Fluorescence of Malignant Tissue," Lancet 2, 436 (1965).
55. R. R. Alfano, D. B. Tata, J. J. Cordero, P. Tomashefsky, F. W. Longo, and M. A. Alfano, "Laser induced fluorescence spectroscopy from native cancerous and normal tissue," IEEE Journal of Quantum Electronics 20, 1507–1511 (1984).
56. N. Ramanujam, "Fluorescence spectroscopy of neoplastic and non-neoplastic tissues," Neoplasia 2, 89–117 (2000).
57. K. Sokolov, M. Follen, and R. Richards-Kortum, "Optical spectroscopy for detection of neoplasia," Curr Opin Chem Biol 6, 651–658 (2002).
58. W. K. Huh, R. M. Cestero, F. A. Garcia, M. A. Gold, R. S. Guido, K. McIntyre-Seltman, D. M. Harper, L. Burke, S. T. Sum, R. F. Flewelling, and R. D. Alvarez, "Optical detection of high-grade cervical intraepithelial neoplasia in vivo: results of a 604-patient study," American Journal of Obstetrics & Gynecology 190, 1249–1257 (2004).
59. S. K. Chang, M. Y. Dawood, G. Staerkel, U. Utzinger, E. N. Atkinson, R. R. Richards-Kortum, and M. Follen, "Fluorescence spectroscopy for cervical precancer detection: Is there variance across the menstrual cycle?," Journal of Biomedical Optics 7, 595–602 (2002).
60. I. Georgakoudi, E. E. Sheets, M. G. Muller, V. Backman, C. P. Crum, K. Badizadegan, R. R. Dasari, and M. S. Feld, "Trimodal spectroscopy for the detection and characterization of cervical precancers in vivo," American Journal of Obstetrics & Gynecology 186, 374–382 (2002).
61. Ramanujam, M. Follen, A. Mahadevan, S. Thomsen, G. Staerkel, A. Malpica, and R. Richards-Kortum, "Cervical pre-cancer detection using a multivariate statistical algorithm based on laser induced fluorescence spectra at multiple excitation wavelengths," Photochem Photobiol 6, 720–735 (1996).
62. J. Wu, M. S. Feld, and R. P. Rava, "Analytical model for extracting intrinsic fluorescence in turbid media," Applied Optics 32, 3585–3595 (1993).
63. G. Zonios, L. Perelman, V. Backman, R. Manoharan, M. Fitzmaurice, J. V. Dam, and M. Feld, "Diffuse reflectance spectroscopy of human adenomatous colon polyps in vivo," Applied Optics 38, 6628–6637 (1999).
64. L. T. Perelman, V. Backman, M. Wallace, G. Zonios, R. Manoharan, A. Nusrat, S. Shields, M. Seiler, C. Lima, T. Hamano, I. Itzkan, J. Van Dam, J. M. Crawford, and M. S. Feld, "Observation of periodic fine structure in reflectance from biological tissue: a new technique for measuring nuclear size distribution," Physical Review Letters 80, 627–630 (1998).
65. S. Lam, T. Kennedy, M. Unger, Y. E. Miller, D. Gelmont, V. Rusch, B. Gipe, D. Howard, J. C. LeRiche, A. Coldman, and A. F. Gazdar, "Localization of bronchial intraepithelial neoplastic lesions by fluorescence bronchoscopy," Chest 113, 696–702 (1998).
66. P. Pierard, J. Faber, J. Hutsebaut, B. Martin, G. Plat, J. P. Sculier, and V. Ninane, "Synchronous lesions detected by autofluorescence bronchoscopy in patients with high-grade preinvasive lesions and occult invasive squamous cell carcinoma of the proximal airways," Lung Cancer 46, 341–347 (2004).
67. K. Haussinger, H. Becker, F. Stanzel, A. Kreuzer, B. Schmidt, J. Strausz, S. Cavaliere, F. Herth, M. Kohlhaufl, K. M. Muller, R. M. Huber, U. Pichlmeier, and T. Bolliger, "Autofluorescence bronchoscopy with white light bronchoscopy

compared with white light bronchoscopy alone for the detection of precancerous lesions: a European randomised controlled multicentre trial," Thorax 60, 496–503 (2005).
68. H. Hoshino, K. Shibuya, M. Chiyo, A. Iyoda, S. Yoshida, Y. Sekine, T. Iizasa, Y. Saitoh, M. Baba, K. Hiroshima, H. Ohwada, and T. Fujisawa, "Biological features of bronchial squamous dysplasia followed up by autofluorescence bronchoscopy," Lung Cancer 46, 187–196 (2004).
69. M. Chiyo, K. Shibuya, H. Hoshino, K. Yasufuku, Y. Sekine, T. Iizasa, K. Hiroshima, and T. Fujisawa, "Effective detection of bronchial preinvasive lesions by a new autofluorescence imaging bronchovideoscope system," Lung Cancer 48, 307–313 (2005).
70. M. Keijzer, R. R. Richards-Kortum, S. L. Jacques, and M. S. Feld, "Fluorescence spectroscopy of turbid media: Autofluorescence of the human aorta," Applied Optics 28, 4286–4292 (1989).
71. S. Avrillier, E. Tinet, D. Ettori, J. M. Tualle, and B. Gelebart, "Influence of the emission-reception geometry in laser-induced fluorescence spectra from turbid media," Applied Optics 37, 2781–2787 (1998).
72. S. Warren, K. Pope, Y. Yazdi, A. J. Welch, S. Thomsen, A. L. Johnston, M. J. Davis, and R. Richards-Kortum, "Combined ultrasound and fluorescence spectroscopy for physico-chemical imaging of atherosclerosis," IEEE Transactions on Biomedical Engineering 42, 121–132 (1995).
73. J. Qu, C. MacAulay, S. Lam, and B. Palcic, "Laser-induced fluorescence spectroscopy at endoscopy: tissue optics, Monte Carlo modeling, and in vivo measurements," Optical Engineering 34, 3334–3343 (1995).
74. J. Y. Qu and J. W. Hua, "Calibrated fluorescence imaging of tissue in vivo," Applied Physics Letters 78, 4040–4042 (2001).
75. S. Warren, K. Pope, Y. Yazdi, A. J. Welch, S. Thomsen, A. L. Johnston, M. J. Davis, and R. Richards-Kortum, "Combined Ultrasound and Fluorescence Spectroscopy for Physico-Chemical Imaging of Atherosclerosis," IEEE Transactions on Biomedical Engineering 42, 121–132 (1995).
76. Q. Zhang, M. G. Muller, J. Wu, and M. S. Feld, "Turbidity-free fluorescence spectroscopy of biological tissue," Optics Letters 25, 1451–1453 (2000).
77. S. K. Chang, D. Arifler, R. Drezek, M. Follen, and R. Richards-Kortum, "Analytical model to describe fluorescence spectra of normal and preneoplastic epithelial tissue: comparison with Monte Carlo simulations and clinical measurements," Journal of Biomedical Optics 9, 511–522 (2004).
78. R. J. McNichols, A. Gowda, B. A. Bell, R. M. Johnigan, K. H. Calhoun, M. Motamedi, "Development of an endoscopic fluorescence image guided OCT probe for oral cancer detection," Proc. SPIE 4254, 23–30, 2001.
79. R. V. Kuranov, V. V. Sapozhnikova, H. M. Shakhova, V. M. Gelikonov, E. V. Zagainova, and S. A. Petrova. "Combined application of optical methods to increase the information content of optical coherent tomography in diagnostics of neoplastic processes." Quantum Electronics 32(11), 993–998 (2002).
80. Z. G. Wang, D. B. Durand, M. Schoenberg, and Y. T. Pan, "Fluorescence guided optical coherence tomography for the diagnosis of early bladder cancer in a rat model," Journal of Urol. 174(6), 2376–81 (2005).
81. U. Utzinger, and R. R. Richards-Kortum, "Fiber optic probes for biomedical optical spectroscopy," Journal of Biomedical Optics 8, 121–147 (2003).
82. S. J. Oldenburg, R. D. Averitt, S. L. Westcott, and N. J. Halas, "Nanoengineering of optical resonances," Chemical Physics Letters 288, 243–247 (1998).

83. G. M. Dobre, A. G. Podoleanu, and R. B. Rosen, "Simultaneous optical coherence tomography–Indocyanine Green dye fluorescence imaging system for investigations of the eye's fundus," Optics Letters 30(1), 58–60 (2005).
84. E. Beaurepaire, L. Moreaux, F. Amblard, and J. Mertz, "Combined scanning optical coherence and two-photon-excited fluorescence spectroscopy," Optics Letters 24, 969–971 (1999).
85. TIE-36 Fluorescence of Optical Glass, in Technical Information, Optics for Devices. 2004, Schott Glass.
86. K. R. Hawkins and P. Yager, "Nonlinear decrease of background fluorescence in polymer thin-films - a survey of materials and how they can complicate fluorescence detection in microTAS," Lab Chip 3(4), 248–52 (2003).
87. M. J. Hodgin, "Epoxies for optoelectronic packaging; applications and material properties," Journal of Microelectronics and Electronic Packaging 1(2), 108–116 (2004).
88. American National Standards Institute, "American National Standard for Safe Use of Lasers," (ANSI, New York, 2000).
89. American Conference of Governmental Industrial Hygienists, "2005 TLVs and BEIs," (ACGIH, Cincinnati, Ohio, 2005).
90. International Commission on Non-Ionizing Radiation Protection, "Guidelines on limits of exposure to laser radiation of wavelengths between 180 nm and 1,000 microm," Health Phys. 71, 804–819 (1996).
91. International Commission on Non-ionizing Radiation Protection, "Revision of guidelines on limits of exposure to laser radiation of wavelengths between 400 nm and 1.4 microm," Health Commission on Non-Ionizing Radiation and Protection, "Guidelines on limits of exp Phys. 79, 431–440 (2000).
92. International Commission on Non-Ionizing Radiation Protection, "Guidelines on limits of exposure to ultraviolet radiation of wavelengths between 180 nm and 400 nm (incoherent optical radiation)," Health Phys. 87, 171–186 (2004).
93. International Commission on Non-Ionizing Radiation and Protection, "Guidelines on limits of exposure to broad-band incoherent optical radiation (0.38 to 3 microm)," Health Phys. 73, 539–554 (1997).
94. Center for Devices and Radiological Health, "Guidance for Industry: Electro-optical Sensors for the In Vivo Detection of Cervical Cancer and its Precursors: Submission Guidance for an IDE/PMA," (US Department of Health and Human Services, New York, 1998).
95. A. F. Fercher, W. Drexler and C. K. Hitzenberger, Optical coherence tomography-principles and applications. Reports on Progress in Physics, 2003. 66(2): pp. 239–303.
96. C. F. Zhu, Q. Liu, and N. Ramanujam, "Effect of fiber optic probe geometry on depth-resolved fluorescence measurements from epithelial tissues: a Monte Carlo simulation," Journal of Biomedical Optics 8, 237–247 (2003).
97. Z. Changfang, L. Quan, and N. Ramanujam, "Effect of fiber optic probe geometry on depth-resolved fluorescence measurements from epithelial tissues: a Monte Carlo simulation," Journal of Biomedical Optics 8, 237–247 (2003).
98. T. J. Pfefer, K. T. Schomacker, M. N. Ediger, and N. S. Nishioka, "Multiple-fiber probe design for fluorescence spectroscopy in tissue," Applied Optics 41, 4712–4721 (2002).
99. T. J. Pfefer, L. S. Matchette, A. M. Ross, and M. N. Ediger, "Selective detection of fluorophore layers in turbid media: the role of fiber-optic probe design," Optics Letters 28, 120–122 (2003).

100. T. J. Pfefer, L. S. Matchette, and R. Drezek, "Influence of illumination-collection geometry on fluorescence spectroscopy in multilayer tissue," Medical & Biological Engineering & Computing 42, 669–673 (2004).
101. J. Wang, P. T. Bender, U. Utzinger, and R. Drezek, "Depth sensitive reflectance measurements using oblique oriented fiber probes," Journal of Biomedical Optics in print (2006).
102. M. C. Skala, G. M. Palmer, C. F. Zhu, Q. Liu, K. M. Vrotsos, C. L. Marshek-Stone, A. Gendron-Fitzpatrick, and N. Ramanujam, "Investigation of fiber-optic probe designs for optical spectroscopic diagnosis of epithelial pre-cancers," Lasers in Surgery and Medicine 34, 25–38 (2004).
103. Q. Liu, and N. Ramanujam, "Experimental proof of the feasibility of using an angled fiber-optic probe for depth-sensitive fluorescence spectroscopy of turbid media," Optics Letters 29, 2034–2036 (2004).
104. T. J. Pfefer, L. S. Matchette, A.M. Ross and M.N. Ediger, "Selective detection of fluorophore layers in turbid media: the role of fiber-optic probe design," Optics Letters 28(2), 120–2 (2003).
105. T. Papaioannou, N. W. Preyer, Q. Y. Fang, A. Brightwell, M. Carnohan, G. Cottone, R. Ross, L. R. Jones and L. Marcu, "Effects of fiber-optic probe design and probe-to-target distance on diffuse reflectance measurements of turbid media: an experimental and computational study at 337 nm," Applied Optics 43(14), 2846–60 (2004).
106. C. Zhu, Q. Liu, and N. Ramanujam, "Effect of fiber optic probe geometry on depth-resolved fluorescence measurements from epithelial tissues: a Monte Carlo simulation," J Biomed Opt 8(2), 237–47 (2003).
107. T. J. Pfefer, K. T. Schomacker, M. N. Ediger and N. S. Nishioka, "Multiple-fiber probe design for fluorescence spectroscopy in tissue," Appl Opt 41(22), 4712–21 (2002).
108. Q. Liu, and N. Ramanujam, "Experimental proof of the feasibility of using an angled fiber-optic probe for depth-sensitive fluorescence spectroscopy of turbid media," Optics Letters 29(17), 2034–6 (2004).
109. M. C. Skala, G. M. Palmer, C. F. Zhu, Q. Liu, K. M. Vrotsos, C. L. Marshek-Stone, A. Gendron-Fitzpatrick and N. Ramanujam, "Investigation of fiber-optic probe designs for optical spectroscopic diagnosis of epithelial pre-cancers," Lasers Surg Med 34(1), 25–38 (2004).
110. R. A. Schwarz, D. Arifler, S. K. Chang, I. Pavlova, I. A. Hussain, V. Mack, B. Knight, R. Richards-Kortum, A. M. Gillenwater, "Ball lens coupled fiber-optic probe for depth-resolved spectroscopy of epithelial tissue," Optics Letters 30(10), 1159–61 (2005).
111. A. M. J. Wang, J. E. Bender, J. Pfefer, U. Utzinger, R. A. Drezek, "Depth-sensitive reflectance measurements using obliquely oriented fiber probes," J Biomed Opt 10(4), 44017 (2005).
112. B. W. Pogue and G. Burke, "Fiber-optic bundle design for quantitative fluorescence measurement from tissue," Applied Optics 37(31), 7429–7436 (1998).
113. P. R. Bargo, S. A. Prahl, and S. L. Jacques, "Optical properties effects upon the collection efficiency of optical fibers in different probe configurations," IEEE Journal on Selected Topics in Quantum Electronics 9(2), 314–321 (2003).
114. J. Barton, F. Guzman, and A. Tumlinson "Dual modality instrument for simultaneous optical coherence tomography imaging and fluorescence spectroscopy," JBO 9(3), 618–623 (2004).

115. J. Y. Qu, Z. Huang, and Jianwen-Hua, "Excitation and collection geometry insensitive fluorescence imaging of tissue-simulating turbid media," Appl. Opt. 39(19), 3344–3356 (2000).
116. A. R. Tumlinson, L. P. Hariri, U. Utzinger, J. K. Barton,"A miniature endoscope for simultaneous OCT-LIF measurement," Applied Optics 43:113–121 (2004).
117. L. P. Hariri, A. R. Tumlinson, D. G. Besselsen, U. Utzinger, E. Gernere, and J. K. Barton, "Endoscopic optical coherence tomography and laser induced fluorescence spectroscopy in murine colon cancer model," Lasers in Surgery and Medicine, in press.
118. J. B. McNally, N. D. Kirkpatrick, L. P. Hariri, A. R. Tumlinson, D. G. Besselsen, E. W. Gerner, U. Utzinger, and J. K. Barton, "Task Based Imaging of Colon Cancer in a Mouse Model (Apc Min/+)," Applied Optics, in press.
119. E. Kanter, R. M. Walker, S. L. Marion, M. Brewer, P. B. Hoyer, and J. K. Barton, "Dual modality imaging of a novel rat model of ovarian carcinogenesis," Journal of Biomedical Optics, in press.
120. N. Ramanujam, M. F. Mitchell, A. Mahadevan, S. Thomsen, A. Malpica, T. Wright, N. Atkinson, and R. Richards-Kortum, "Development of a multivariate statistical algorithm to analyze human cervical tissue fluorescence spectra acquired in vivo," Lasers in Surgery & Medicine 19, 46–62 (1996).
121. E. Svistun, R. Alizadeh-Naderi, A. El-Naggar, R. Jacob, A. Gillenwater, and R. Richards-Kortum, "Vision enhancement system for detection of oral cavity neoplasia based on autofluorescence," Head & Neck 26, 205–215 (2004).
122. U. Utzinger, M. Bueeler, S. Oh, D. L. Heintzelman, E. S. Svistun, M. Abd-El-Barr, A. Gillenwater, and R. Richards-Kortum, "Optimal visual perception and detection of oral cavity neoplasia," IEEE Transactions on Biomedical Engineering 50, 396–399 (2003).
123. M. G. Muller, T. A. Valdez, I. Georgakoudi, V. Backman, C. Fuentes, S. Kabani, N. Laver, Z. Wang, C. W. Boone, R. R. Dasari, S. M. Shapshay, and M. S. Feld, "Spectroscopic detection and evaluation of morphologic and biochemical changes in early human oral carcinoma," Cancer 97, 1681–1692 (2003).
124. D. L. Heintzelman, U. Utzinger, H. Fuchs, A. Zuluaga, K. Gossage, A. M. Gillenwater, R. Jacob, B. Kemp, and R. R. Richards-Kortum, "Optimal excitation wavelengths for in vivo detection of oral neoplasia using fluorescence spectroscopy," Photochemistry & Photobiology 72, 103–113 (2000).
125. C. Zhu, G. M. Palmer, T. M. Breslin, F. Xu, and N. Ramanujam, "Use of a multiseparation fiber optic probe for the optical diagnosis of breast cancer," Journal of Biomedical Optics 10, 024032 (2005).
126. G. M. Palmer, C. Zhu, T. M. Breslin, F. Xu, K. W. Gilchrist, and N. Ramanujam, "Comparison of multiexcitation fluorescence and diffuse reflectance spectroscopy for the diagnosis of breast cancer," IEEE Transactions on Biomedical Engineering 50, 1233–1242 (2003).
127. T. M. Breslin, F. Xu, G. M. Palmer, C. Zhu, K. W. Gilchrist, and N. Ramanujam, "Autofluorescence and diffuse reflectance properties of malignant and benign breast tissues," Annals of Surgical Oncology 11, 65–70 (2004).
128. P. K. Gupta, S. K. Majumder, and A. Uppal, "Breast cancer diagnosis using N2 laser excited autofluorescence spectroscopy," Lasers in Surgery & Medicine 21(5), 417–422 (1997).

129. K. T. Schomacker, J. K. Frisoli, C. C. Compton, T. J. Flotte, J. M. Richter, N. S. Nishioka, and T. F. Deutsch, "Ultraviolet laser-induced fluorescence of colonic tissue: basic biology and diagnostic potential," Lasers in Surgery & Medicine 12, 63–78 (1992).
130. T. J. Pfefer, D. Y. Paithankar, J. M. Poneros, K. T. Schomacker, and N. S. Nishioka, "Temporally and spectrally resolved fluorescence spectroscopy for the detection of high grade dysplasia in Barrett's esophagus," Lasers in Surgery and Medicine 32, 10–16 (2003).
131. M. A. Ortner, B. Ebert, E. Hein, K. Zumbusch, D. Nolte, U. Sukowski, J. Weber-Eibel, B. Fleige, M. Dietel, M. Stolte, G. Oberhuber, R. Porschen, B. Klump, H. Hortnagl, H. Lochs, and H. Rinneberg, "Time gated fluorescence spectroscopy in Barrett's oesophagus," Gut 52, 28–33 (2003).
132. F. Koenig, F. J. McGovern, H. Enquist, R. Larne, T. F. Deutsch, and K. T. Schomacker, "Autofluorescence guided biopsy for the early diagnosis of bladder carcinoma," Journal of Urology 159, 1871–1875 (1998).
133. W. C. Lin, S. A. Toms, M. Johnson, E. D. Jansen, and A. Mahadevan-Jansen, "In vivo brain tumor demarcation using optical spectroscopy," Photochemistry & Photobiology 73, 396–402 (2001).
134. A. Sivaramakrishnan and D. Graupe, "Brain tumor demarcation by applying a LAMSTAR neural network to spectroscopy data," Neurological Research 26, 613–621 (2004).
135. W. Drexler, U. Morgner, F. X. Kartner, C. Pitris, S. A. Boppart, X. D. Li, E. P. Ippen, and J. G. Fujimoto, "In vivo ultrahigh-resolution optical coherence tomography," Optics Letters 24, 1221–1223 (1999).
136. B. E. Bouma, G. J. Tearney, I. P. Bilinsky, B. Golubovic, and J. G. Fujimoto, "Self-phase-modulated Kerr-lens mode-locked Cr:forsterite laser source for optical coherence tomography," Optics Letters 21, 1839–1841 (1996).
137. I. Hartl, X. D. Li, C. Chudoba, R. K. Ghanta, T. H. Ko, J. G. Fujimoto, J. K. Ranka, and R. S. Windeler, "Ultrahigh-resolution optical coherence tomography using continuum generation in an air-silica microstructure optical fiber," Optics Letters 26, 608–610 (2001).
138. N. D. Kirkpatrick, C. P. Zou, M. A. Brewer, W. R. Brands, R. A. Drezek, and U. Utzinger, "Endogenous fluorescence spectroscopy of cell suspensions for chemopreventive drug monitoring," Photochemistry and Photobiology 81, 125–134 (2005).
139. M. Bruchez, M. Moronne, P. Gin, S. Weiss, and A. P. Alivisatos, "Semiconductor nanocrystals as fluorescent biological labels," Science 281, 2013–2016 (1998).
140. A. M. Smith, and S. Nie, "Chemical analysis and cellular imaging with quantum dots," Analyst 129, 672–677 (2004).
141. J. M. Dixon, M. Taniguchi, and J. S. Lindsey, "PhotochemCAD 2: A refined program with accompanying spectral databases for photochemical calculations," Photochem. Photobiol. 81, 212–213 (2005).
142. R. C. Benson, and H. A. Kues, "Fluorescence Properties of Indocyanine Green as Related to Angiography," Phys. Med. Biol. 23, 159–163 (1978).